which are characteristic of Fe^{2+} four-coordinate square-planar geometry. The apparent resolution of the pre-edge peak (due to a $1s \rightarrow 4p_z$ electronic transition) for the reduced, adsorbed macrocycle is clearly less than that for either crystalline FePc (recorded under the same experimental conditions) or iron *meso*-tetrakis(phenyl)porphyrin.[12] There are at least two plausible explanation for this effect: (i) a multiplicity of closely related iron environments (all with 4-fold square-planar coordination) due to structural distortions of the TMPP framework upon adsorption and reduction of the parent macrocycle and (ii) a heterogeneity of coordination, such that the principal fraction of iron in the reduced, adsorbed macrocycle is four-coordinate square-planar and a small fraction is five- or six-coordinate with distant axial ligands. The latter would be the case if, for example, some of the adsorbed material is not in either electronic or electrolytic contact with the rest of the system. Nevertheless, upon polarizing the electrode at a potential positive enough to reoxidize the adsorbed FeTMPP, the XANES data obtained were essentially identical to those shown in curve B, Figure 3, for the fully oxidized $(FeTMPP)_2O$/BP complex. This indicates that, to the level of sensitivity of the measurements, the redox process is reversible. This may be regarded as rather surprising in view of the large structural rearrangements associated with the reformation of the μ-oxo framework.

Experiments conducted in solutions of 0.05 M H_2SO_4 (pH = 1) and 0.0015 M NaOH, 0.05 M H_3BO_3, and 0.05 M Na_2SO_4 (pH = 8.7), for which XANES were recorded at intermediate potentials (see supplementary material), were characterized by the presence of at least two isosbestic points, as would be expected for the interconversion of one species into the other.

Conclusions

The in situ iron XANES described herein provides conclusive evidence, for the first time, that the coordination about Fe^{2+} in the supported, fully reduced macrocycle is remarkably different from that about Fe^{3+} in the corresponding fully oxidized macrocycle. It is thus concluded from the iron K-edge XANES results that $(FeTMPP)_2O$ in the adsorbed state retains its μ-oxo character and undergoes a two-electron reduction to yield predominantly axially uncoordinated FeTMPP. This assignment is in agreement with earlier in situ ^{57}Fe Mossbauer effect measurements on the same system in which the isomer shift and quadrupole splitting of the reduced species observed at about 250 K were consistent with those of a ferrous porphyrin species.[5]

Acknowledgment. This work was supported by the Gas Research Institute. Research was carried out (in part) at the National Synchrotron Light Source, Brookhaven National Laboratory, which is supported by the U.S. Department of Energy, Division of Materials Sciences and Division of Chemical Sciences (DOE Contract No. DE-AC02-76CH0016).

Supplementary Material Available: Plot of F/I_0 vs energy for normalized iron K-edge fluorescence XANES data (1 page). Ordering information is given on any current masthead page.

Chemical and Spectroscopic Studies of the Mixed-Valent Derivatives of the Non-Heme Iron Protein Hemerythrin

James M. McCormick, Richard C. Reem, and Edward I. Solomon*

Contribution from the Department of Chemistry, Stanford University, Stanford, California 94305.
Received August 20, 1990

Abstract: The electronic transitions of the mixed-valent [Fe(II), Fe(III)] form of the binuclear non-heme iron protein hemerythrin are assigned using absorbance, circular dichroism, and low-temperature magnetic circular dichroism (MCD) spectroscopies. $^1/_2Met_r$ (prepared by reduction of met) and the ligand bound forms are found to have both irons in octahedral ligand geometries, while for $^1/_2met_o$ (prepared by oxidation of deoxy) the Fe^{2+} is five-coordinate and the Fe^{3+} is six-coordinate. Variable-temperature MCD and EPR spectroscopies are used to probe the ground-state magnetic properties; all $^1/_2$met forms are found to have $J \approx -8$ cm^{-1}, consistent with an endogenous bridging OH^-. $^1/_2Met_r$ and $^1/_2met_o$ are found to be in a pH-dependent equilibrium, reflecting binding of OH^- as an exogenous ligand. The differences in geometric and electronic structure between $^1/_2met_r$ and $^1/_2met_o$ are related to the redox reactivity of this active site.

Introduction

A coupled binuclear non-heme iron active site occurs in a variety of different enzymes and proteins whose function often involves reaction with dioxygen. Members of this class of proteins (and their dioxygen reactivities) include the following: hemerythrin (Hr, oxygen transport and storage),[1] ribonucleotide diphosphate reductase (RDPR, formation of a catalytically active tyrosine radical),[2] methane monooxygenase (MMO, activation of dioxygen for insertion into carbon-hydrogen bonds),[3] the purple acid phosphatases (PAP, inactivated by dioxygen in the presence of phosphate),[4] and rubrerythrin (Rb, unknown).[5] The binuclear iron site can exist in three oxidation states: met [Fe(III), Fe(III)], $^1/_2$met (or semimet) [Fe(II), Fe(III)], and deoxy (or fully reduced) [Fe(II), Fe(II)]. All three oxidation states can be obtained for

(1) (a) Wilkins, P. C.; Wilkins, R. G. *Coord. Chem. Rev.* **1987**, *79*, 195-214. (b) Klotz, I. M.; Kurtz, D. M., Jr. *Acc. Chem. Res.* **1984**, *17*, 16-22.

(2) (a) Stubbe, J. *J. Biol. Chem.* **1990**, *265*, 5329-5332. (b) Sjöberg, B.-M.; Gräslund, A. Ribonucleotide Reductase. In *Advances in Inorganic Biochemistry Vol. 5*; Theil, E. C., Eichorn, G. L., Marzilli, L. G., Eds.; Elsevier: 1983; pp 87-110. (c) Reichard, P.; Ehrenberg, A. *Science* **1983**, *221*, 514-519.

(3) (a) Dalton, H. Oxidation of Hydrocarbons by Methane Monooxygenase from a Variety of Microbes. In *Advances in Applied Microbiology*; Umbreit, W. W., Ed.; Academic Press: 1980; pp 71-87. (b) Fox, B. G.; Froland, W. A.; Dege, J. B.; Lipscomb, J. D. *J. Biol. Chem.* **1989**, *264*, 10023-10033.

(4) Doi, K.; Antanaitis, B. C.; Aisen, P. The Binuclear Iron Centers of Uteroferrin and the Purple Acid Phosphatases. In *Structure and Bonding 70*; Springer-Verlag: Berlin, 1988; pp 1-26.

(5) LeGall, B. G.; Prickril, B. C.; Moura, I.; Xavier, A. V. *Biochemistry* **1988**, *27*, 1636-1642.

0002-7863/91/1513-9066$02.50/0

Hr and MMO,[1,3] but RDPR has no characterized $^1/_2$met form.[2] Met and $^1/_2$met forms of PAP are accessible, but PAP is different from the other binuclear non-heme iron proteins in that it is active in the $^1/_2$met form.[4]

Hr was the first characterized binuclear non-heme iron protein[1,6] and has served as a system on which to define spectral methods.[7,8] Most Hrs are octameric and do not bind oxygen cooperatively; however, instances of monomeric and trimeric Hr[9] as well as cooperative oxygen binding are known.[10] Spectroscopic studies on the met forms of Hr have shown that both Fe^{3+} are high spin with the large antiferromagnetic exchange coupling (for metHr $J = -134$ cm^{-1} using $\hat{H} = -2JS_1 \cdot S_2$)[11] mediated by a μ-oxo endogenous bridge.[12] The 2.0-Å crystal structure of metHr confirmed the presence of the oxo as well as two carboxylate bridges.[13] The crystal structure also shows that one Fe is six-coordinate with three histidines in addition to the bridging ligands (3-His Fe), and the other is five-coordinate with two histidines completing the coordination sphere (2-His Fe). Exogenous ligands bind to the 2-His Fe making it six-coordinate, giving the metL$^-$ derivatives ($L^- = N_3^-$, Cl^-, Br^-, OH^-, SCN^-, F^-, etc.).[8,12-14,15]

For deoxyHr a combination of circular dichroism (CD), near-IR absorbance (NIR ABS), and variable-temperature magnetic circular dichroism (VT MCD) spectroscopic studies have shown that the site has one six- and one five-coordinate Fe^{2+} and a much lower antiferromagnetic exchange coupling ($12 \leq -J \leq 38$ cm^{-1}) than metHr.[7] The lower exchange coupling has been interpreted as indicating protonation of the oxo bridge in metHr to a hydroxo bridge. The coordination geometries of the irons in deoxyHr have been confirmed by an electron difference map between deoxy and metHr.[16] Several small molecules (N_3^-, F^-, OCN^-) bind to the deoxyHr site at the five-coordinate Fe^{2+}, making it six-coordinate. The exchange interaction is perturbed such that the Fe^{2+} are ferromagnetically coupled which is proposed to be the result of further protonation of the bridge to H_2O.[7]

The redox chemistry of met and deoxyHr through the $^1/_2$met oxidation level has been well-studied, as different intermediates are generated depending on the method of preparation.[17-24] The rapid ($k_1 \approx 10^5$ M^{-1} s^{-1}) reduction of met and metOH$^-$ leads to $^1/_2$met$_r$,[17-19] which is characterized by a rhombic EPR spectrum.[20a] Further reduction to deoxy is biphasic and very slow ($k_2 \approx 10^{-3}$ s^{-1}, $k_3 \approx 10^{-4}$ s^{-1}).[17-19,21] The rate constant k_2 has been shown to have a complicated pH dependence, with the highest rates at low and high pH with a minimum rate near pH 7.[18] While $^1/_2$met$_r$ is only slowly reduced, it is rapidly oxidized.[17,18,22,23] Oxidation of deoxy gives $^1/_2$met$_o$,[24-26] which has an axial EPR spectrum.[20a] While the rate of further oxidation of $^1/_2$met$_o$ is slow, the reduction of $^1/_2$met$_o$ to deoxy is very fast.[22,23,27] In contrast to the reduction of $^1/_2$met$_r$ the oxidation of $^1/_2$met$_o$ has a simple pH dependence (fastest at high pH and slowest at low pH).[25] Wilkins first proposed a mechanism involving disproportionation via long distance electron transfer between iron sites within the octamer to account for the observed redox kinetics.[17a] Further study of the kinetics concluded that $^1/_2$met$_r$ and $^1/_2$met$_o$ are also interconverted.[17b-g,18,19,23,24] We have proposed this interconversion, and the different reactivities of $^1/_2$met$_r$ and $^1/_2$met$_o$ are due to a bound exogenous OH^- in $^1/_2$met$_r$ which is not present in $^1/_2$met$_o$.[28]

The $^1/_2$metHr site has been characterized by several spectral methods, which have focused on the relatively stable $^1/_2$metN_3^-. Paramagnetic NMR ($^1/_2$metN_3^-),[29] temperature-dependent EPR ($^1/_2$metN_3^-, $^1/_2$met$_r$),[19] and VT MCD ($^1/_2$met$_r$, $^1/_2$met$_o$)[28] have shown the $^1/_2$met site to be weakly antiferromagnetically coupled ($J \approx -10$ cm^{-1}), consistent with the presence of a OH^- bridge. EXAFS on $^1/_2$metN_3^- has also indicated that the μ-oxo bridge

(6) (a) Okamura, M. Y.; Klotz, I. M. *Inorganic Biochemistry*; Eichorn, G. L. Ed.; Elsevier: 1973; pp 320-343. (b) Kurtz, D. M., Jr.; Shriver, D. F.; Klotz, I. M. *Coord. Chem. Rev.* **1977**, *24*, 145-178. (c) Klippenstein, G. L. *Am. Zool.* **1980**, *20*, 39-51.

(7) (a) Reem, R. C.; Solomon, E. I. *J. Am. Chem. Soc.* **1984**, *106*, 8323-8325. (b) Reem, R. C.; Solomon, E. I. *J. Am. Chem. Soc.* **1987**, *109*, 1216-1226.

(8) Reem, R. C.; McCormick, J. M.; Richardson, E. E.; Devlin, F. J.; Stephens, P. J.; Musselman, R. L.; Solomon, E. I. *J. Am. Chem. Soc.* **1989**, *111*, 4688-4704.

(9) (a) Klippenstein, G. L.; Van Riper, D. A.; Oosterom, E. A. *J. Biol. Chem.* **1972**, *18*, 5959-5963. (b) Joshi, J. G.; Sullivan, B. *Comp. Biochem. Physil.* **1973**, *44B*, 857-867. (c) Liberatore, F. A.; Truby, M. F.; Klippenstein, G. L. *Arch. Biochem. Biophys.* **1974**, *160*, 223-229. (d) Addison, A. W.; Bruce, R. E. *Arch. Biochem. Biophys.* **1977**, *183*, 328-332. (e) Wells, R. M. G. *N. Z. J. Zool.* **1982**, *9*, 243-248. (f) Addison, A. W.; Dougherty, P. L. *Comp. Biochem. Physiol.* **1982**, *72B*, 433-438.

(10) (a) Manwell, C. *Science* **1960**, *132*, 550-551. (b) Richardson, D. E.; Reem, R. C.; Solomon, E. I. *J. Am. Chem. Soc.* **1983**, *105*, 7780-7781. (c) Richardson, D. E.; Emad, M.; Reem, R. C.; Solomon, E. I. *Biochemistry* **1987**, *26*, 1003-1013.

(11) Schugar, H. J.; Rossman, G. R.; Barraclogh, C. G.; Gray, H. B. *J. Am. Chem. Soc.* **1972**, *94*, 2683-2690.

(12) (a) Hendrickson, W. A.; Co, M. S.; Smith, J. L.; Hodgson, K. O.; Klippenstein, G. L. *Proc. Natl. Acad. Sci. U.S.A.* **1982**, *79*, 6255-6259. (b) Elam, W. T.; Stern, E. A.; McCallum, J. D.; Sanders-Loehr, J. *J. Am. Chem. Soc.* **1982**, *104*, 6369-6373. (c) Elam, W. T.; Stern, E. A.; McCallum, J. D.; Sanders-Loehr, J. *J. Am. Chem. Soc.* **1983**, *105*, 1919-1923. (d) Zhang, K.; Stern, E. A.; Ellis, F.; Sanders-Loehr, J.; Shiemke, A. K. *Biochemistry* **1988**, *27*, 7470-7479. (e) Kurtz, D. M., Jr.; Shriver, D. F.; Klotz, I. M. *J. Am. Chem. Soc.* **1976**, *98*, 5033-5035. (f) Freier, S. M.; Duff, L. L.; Shriver, D. F.; Klotz, I. M. *Arch. Biochem. Biophys.* **1980**, *205*, 449-463. (g) McCallum, J. D.; Shiemke, A. K.; Sanders-Loehr, J. *Biochemistry* **1984**, *106*, 4951-4956. (h) Shiemke, A. K.; Loehr, T. M.; Sanders-Loehr, J. *J. Am. Chem. Soc.* **1984**, *106*, 4951-4956. (i) Shiemke, A. K.; Loehr, T. M.; Sanders-Loehr, J. *J. Am. Chem. Soc.* **1986**, *108*, 2437-2443. (j) Gay, R. R.; Solomon, E. I. *J. Am. Chem. Soc.* **1978**, *111*, 1972-1973.

(13) Stenkamp, R. E.; Sieker, L. C.; Jensen, L. H. *J. Am. Chem. Soc.* **1984**, *106*, 618-622.

(14) Grabett, K.; Darnall, D. W.; Klotz, I. M.; Williams, R. J. P. *Arch. Biochem. Biophys.* **1969**, *135*, 419-434.

(15) The low pH form of [Fe(III), Fe(III)] Hr, previously referred to as met"aquo",[14] has one six- and one five-coordinate Fe^{3+} and is referred to as met, while the high pH form is referred to as metOH$^-$ in this study.

(16) Stenkamp, R. E.; Sieker, L. C.; Jensen, L. H.; McCallum, J. D.; Sanders-Loehr, J. *Proc. Natl. Acad. Sci. U.S.A.* **1985**, *82*, 713-716.

(17) (a) Harrington, P. C.; Wilkins, R. G. *J. Biol. Chem.* **1979**, *254*, 7505-7508. (b) Bradič, Z.; Harrington, P. C.; Wilkins, R. G. *Biochemistry* **1979**, *18*, 889-893. (c) Bradič, Z.; Harrington, P. C.; Wilkins, R. G.; Yoneda, G. *Biochemistry* **1980**, *19*, 4149-4155. (d) Harrington, P. C.; Wilkins, R. G. *J. Am. Chem. Soc.* **1981**, *103*, 1550-1556. (e) Armstrong, F. A.; Harrington, P. C.; Wilkins, R. G. *J. Inorg. Biochem.* **1979**, *11*, 205-212. (f) Harrington, P. C.; Muhoberac, B. B.; Wharton, D. C.; Wilkins, R. G. *Biochemistry* **1981**, *20*, 6134-6139. (g) Harrington, P. C.; deWaal, D. J. A.; Wilkins, R. G. *Arch. Biochem. Biophys.* **1978**, *191*, 444-451.

(18) (a) Armstrong, G. D.; Ramasami, T.; Sykes, A. G. *J. Chem. Soc., Chem. Commun.* **1981**, 1017-1019. (b) Armstrong, G. D.; Ramasami, T.; Sykes, A. G. *Inorg. Chem.* **1985**, *24*, 3230-3234. (c) Armstrong, G. D.; Sykes, A. G. *Inorg. Chem.* **1986**, *25*, 3725-3729. (d) Armstrong, G. D.; Sykes, A. G. *Inorg. Chem.* **1986**, *25*, 3514-3516.

(19) Pearce, L. L.; Kurtz, D. M., Jr.; Xia, Y.-M.; Debrunner, P. G. *J. Am. Chem. Soc.* **1987**, *109*, 7286-7293.

(20) (a) Muhoberac, B. B.; Wharton, D. C.; Babcock, L. M.; Harrington, P. C.; Wilkins, R. G. *Biochim. Biophys. Acta* **1980**, *626*, 337-345. (b) Antanaitis, B. C.; Aisen, P. *J. Biol. Chem.* **1982**, *257*, 1855-1859. (c) Antanaitis, B. C.; Aisen, P. *J. Biol. Chem.* **1982**, *257*, 5330-5332. (d) Woodland, M. P.; Patil, D. S.; Cammack, R.; Dalton, H. *Biochim. Biophys. Acta* **1986**, *873*, 237-242.

(21) In the presence of excess reductant, the second stage is characterized by the loss of $^1/_2$met$_r$ and the production of deoxy and met. In addition, Kurtz et al. have presented Mössbauer evidence[19] that the [Fe(III), Fe(III)] species formed in the second stage of reduction is not the normal met.

(22) The rate of oxidation for $^1/_2$met$_r$ from *P. gouldii* is 3.4×10^2 M^{-1} s^{-1}, and for $^1/_2$met$_r$ from *T. zostericola* the rate is 4.0×10^5 M^{-1} s^{-1} at pH 8.2 and $K_3Fe(CN)_6$ as the oxidant.[23]

(23) Wilkins, R. G.; Harrington, P. C. The Chemistry of Hemerythrin. In *Advances in Inorganic Biochemistry Vol. 5*; Theil, E. C., Eichorn, G. L., Marzilli, L. G., Eds.; Elsevier: 1983; pp 51-85.

(24) Babcock, L. M.; Bradič, Z.; Harrington, P. C.; Wilkins, R. G.; Yoneda, G. S. *J. Am. Chem. Soc.* **1980**, *102*, 2849-2850.

(25) Armstrong, G. D.; Sykes, A. G. *Inorg. Chem.* **1987**, *26*, 3392-3398.

(26) There are differences in reactivity for Hr from different species.[23] In some instances the oxidation is further complicated, by binding of the oxidant to the protein.[24,25]

(27) The redox reactivity of $^1/_2$met$_o$ is different depending on the species from which the Hr was obtained.[23] With $K_3Fe(CN)_6$, $^1/_2$met$_o$ from *P. gouldii* is oxidized at a rate of 1.7×10^2 M^{-1} s^{-1} at pH 6.3, but $^1/_2$met$_o$ from *T. zostericola* is oxidized at a rate of 6.1×10^{-4} s^{-1} at pH 6.3. $^1/_2$Met$_o$ is reduced to deoxy at $\sim 10^5$ M^{-1} s^{-1} at pH 8.2.[23]

(28) McCormick, J. M.; Solomon, E. I. *J. Am. Chem. Soc.* **1990**, *112*, 2005-2007.

(29) (a) Maroney, M. J.; Lauffer, R. B.; Que, L., Jr. *J. Am. Chem. Soc.* **1984**, *106*, 6445-6446. (b) Maroney, M. J.; Kurtz, D. M., Jr.; Nocek, J. M.; Pearce, L. L.; Que, L., Jr. *J. Am. Chem. Soc.* **1986**, *108*, 6871-6879.

in metN$_3^-$ is no longer present in $^1/_2$metN$_3^-$.[30] The EPR spectrum of the $^1/_2$met species is characteristic of the coupled binuclear non-heme iron center; all three dimer g values are less than 2.00, indicating a high-spin Fe^{3+} ($S = {}^5/_2$) is antiferromagnetically coupled to a high-spin Fe^{2+} ($S = 2$) resulting in an $S_{tot} = {}^1/_2$ ground state.[3b,4,5,20] $^1/_2$MetN$_3^-$Hr has been shown to be a localized class II mixed-valent system[31] by Raman[32] and paramagnetic NMR,[28] with the presence of N_3^- to Fe^{3+} ligand-to-metal charge-transfer bands (LMCT) demonstrating the N_3^- is bound to the Fe^{3+}.[32] With a class II system the spectroscopic properties of mononuclear high-spin Fe^{2+} and Fe^{3+} must be considered.

High-spin d^6 Fe^{2+} in an octahedral ligand field has a $^5T_{2g}$ ground state with a ^5E_g excited state at $10Dq_{O_h}$ ($\sim$10 000 cm^{-1}). A Jahn–Teller distortion or low site symmetry splits the ^5E_g excited state (Δ^5E) by $\sim$2000 cm^{-1}.[33] In the five-coordinate geometries the ^5E_g state is split to a greater extent than in an octahedral geometry, with $\Delta^5E \geq \sim$5000 cm^{-1}.[34] For tetrahedral Fe^{2+} coordination $10Dq_{T_d}$ is $-{}^4/_9\ 10Dq_{O_h}$ so the ground state is ^5E and the excited state is $^5T_2$. The spin allowed ligand field transition for a tetrahedral site will then occur at $\sim$5000 cm^{-1}.[35]

High-spin Fe^{3+} will have a $^6A_1$ ground state in all coordination geometries, and, as there are no sextet ligand field excited states possible in d^5, all the ligand field transitions will be spin forbidden. The two lowest energy ligand field transitions are the $^6A_1 \rightarrow {}^4T_1$ and $^6A_1 \rightarrow {}^4T_2$, both of which shift to higher energy with decreasing ligand field strength. Thus, ligand field transitions occur at highest energy for tetrahedral Fe^{3+} ($^6A_1 \rightarrow {}^4T_1$ 16 500–18 100 cm^{-1}, $^6A_1 \rightarrow {}^4T_2$ 19 900–20 900 cm^{-1}), at lowest energy for octahedral ($^6A_1 \rightarrow {}^4T_1$ 7200–11 400 cm^{-1}, $^6A_1 \rightarrow {}^4T_2$ 12 000–15 800 cm^{-1}), and at intermediate energies for five-coordinate geometries ($^6A_1 \rightarrow {}^4T_1$ 7500–14 000 cm^{-1}, $^6A_1 \rightarrow {}^4T_2$ 16 100–20 100 cm^{-1}).[36] The orbital degeneracy of the ^4T states can be split by low symmetry into as many as three transitions. A third Fe^{3+} ligand field transition will also be of importance here, the ligand field independent $^6A_1 \rightarrow {}^4A_1, {}^4E$ at $\sim$20 000 cm^{-1}. Its energy reflects only electron repulsion, and thus it can be used to obtain information on covalency in the Fe^{3+} complex. Fe^{3+} complexes often exhibit intense LMCT transitions at energies above $\sim$20 000 cm^{-1} (Fe^{2+} LMCT are at much higher energy) and can provide an additional means of probing the Fe^{3+} center.

In addition to the ligand field transitions and LMCT, a class II mixed-valent Fe^{2+}–Fe^{3+} dimer can have an intervalent transfer (IT) transition involving the optical excitation of the extra electron on the Fe^{2+} to the Fe^{3+}. IT transitions are usually identified by their presence only in the mixed-valent form of a metal dimer.[37] An IT band will be predominantly polarized only along the metal–metal vector and is expected to have weak MCD intensity at low temperature.[38] This arises from the selection rule for MCD C-term intensity ($I \propto g_x m_y m_z + g_y m_x m_z + g_z m_x m_y$) which requires two perpendicular transition dipole moments (m_i, $i = x, y, z$).

In this study the iron centers in the $^1/_2$metHr active site are probed using a combination of excited-state spectral methods (ABS, CD, and LT MCD) in both the ligand field (and IT) region from 5000 to $\sim$20 000 cm^{-1} and the LMCT region from $\sim$20 000 to $\sim$33 000 cm^{-1}. The dimer ground-state magnetic structure has been defined by VT MCD in conjunction with EPR and variable field MCD. Together these methods allow a direct probe of the coordination geometries of both the Fe^{2+} and the Fe^{3+} as well as the interactions between the metal centers in the dimer and hence bridging ligation. These studies have been pursued on $^1/_2$met$_o$, $^1/_2$met$_r$, and $^1/_2$metL$^-$ (L$^-$ = OCN$^-$, Cl$^-$, Br$^-$, SCN$^-$, CN$^-$, and N$_3^-$) and provide significant insight into the geometric and electronic structure contributions to the redox reactivities of this active site.

Experimental Section

Hr was isolated from live *Phascolopsis gouldii* obtained from the Marine Biological Laboratory, Woods Hole, MA following the published procedure except for the N$_3^-$ dialysis and crystallization steps.[39] The oxyHr was extensively dialyzed against 0.10 M Tris(SO$_4^{2-}$)[40] pH 7.70 and concentrated to $\sim$5 mM for storage in liquid N$_2$ or prepared for subsequent experiments.[41]

Stock metHr samples were prepared by dialysis of oxyHr against $\sim$6 mM K$_3$Fe(CN)$_6$ overnight in 0.1 M Tris(SO$_4^{2-}$) pH 7.70 at 4 °C, with two buffer changes. For experiments at other pHs, metHr was dialyzed into either 0.1 M MES pH 6.00, 0.1 M HEPES pH 7.00 (or pH 8.20), or 0.1 M CHES pH 9.00 (all buffers from Sigma).[42,43] Buffers were made 0.15 ([Hr] < $\sim$4 mM) or 0.30 M ([Hr] > $\sim$4 mM) in Na$_2$SO$_4$ (Baker).[44] The concentration of met between pH $\sim$7 and $\sim$8 was determined by conversion to metN$_3^-$ (ϵ_{446nm} = 3700 M^{-1} cm^{-1})[14] with a small volume of 5.0 M NaN$_3$. Outside this pH range, ϵ values of met or metOH$^-$ were used.[14] Stock deoxyHr samples were prepared by anaerobic dialysis of oxyHr (concentrated beforehand) against $\sim$10 mM Na$_2$S$_2$O$_4$ in one of the buffers described above at 4 °C for 24 h followed by three changes of anaerobic buffer. The deoxy concentration was checked by conversion to oxy (ϵ_{500nm} = 2200 M^{-1} cm^{-1}),[14] by exposure to air, and by the deoxy CD band ($\Delta\epsilon_{1070nm}$ = +0.44 M^{-1} cm^{-1}).[7] The concentration of the stock samples for the different spectroscopic techniques were 12–15 mM for NIR ABS, CD, and MCD and 2–10 mM for all other experiments. For NIR experiments the Hr samples were deuterated by anaerobic dialysis of an $\sim$1.0-mL stock deoxyHr or metHr ($\sim$15 mM) against $\sim$20 mL of buffer in D$_2$O, with two buffer changes. The final dialysis solution was used as the reference sample for the NIR ABS and CD experiments. All other reagents were prepared in fresh D$_2$O.

$^1/_2$Met$_r$ was prepared from met in the ABS or CD cuvettes under anaerobic conditions at room temperature by addition of 1 equiv of Na$_2$S$_2$O$_4$. Met samples were made oxygen free by anaerobic dialysis at 4 °C for 24 h. The Na$_2$S$_2$O$_4$ concentration was checked by titration with standard K$_3$Fe(CN)$_6$ (ϵ_{420nm} = 1010 M^{-1} cm^{-1}).[19] $^1/_2$Met$_o$ samples were anaerobically prepared in situ by addition of 1 equiv of K$_3$Fe(CN)$_6$ to deoxyHr at room temperature. $^1/_2$MetL$^-$ samples were prepared from $^1/_2$met$_o$ and $^1/_2$met$_r$ by addition of 20–50 μL of concentrated anion solutions to freshly prepared $^1/_2$met samples giving anion concentrations of $\sim$0.1–0.2 M.[45] $^1/_2$Met$_r$ and $^1/_2$met$_o$ formation was quantitated by

(30) Scarrow, R. C.; Maroney, M. J.; Palmer, S. M.; Que, L., Jr.; Roe, A. L.; Salowe, S. P.; Stubbe, J. *J. Am. Chem. Soc.* **1987**, *109*, 7857–7864.
(31) Robin, M. B.; Day, P. *Adv. Inorg. Radiochem.* **1967**, *10*, 247–422.
(32) Irwin, M. J.; Duff, L. L.; Shriver, D. F.; Klotz, I. M. *Arch. Biochem. Biophys.* **1983**, *224*, 473–478.
(33) (a) Cotton, F. A.; Meyers, M. D. *J. Am. Chem. Soc.* **1960**, *82*, 5023. (b) Goodgame, D. M. L.; Goodgame, M.; Hitchman, M. A.; Weeks, M. J. *Inorg. Chem.* **1966**, *5*, 635. (c) Bubridge, C. D.; Goodgame, D. M. L. *Inorg. Chim. Acta* **1970**, *4*, 231–234. (d) Sanders-Loehr, J.; Loehr, T. M.; Mauk, A. G.; Gray, H. B. *J. Am. Chem. Soc.* **1980**, *103*, 6992–6996.
(34) (a) Goedken, V. L.; Merrell, P. H.; Busch, D. H. *J. Am. Chem. Soc.* **1972**, *94*, 3397–3405. (b) Ciampolini, M.; Nardi, N. *Inorg. Chem.* **1966**, *5*, 1150–1154. (c) Riley, D. P.; Merrell, P. H.; Stone, J. A.; Busch, D. H. *Inorg. Chem.* **1975**, *14*, 490–494.
(35) Forster, D.; Goodgame, D. M. L. *J. Chem. Soc.* **1964**, 454–458.
(36) (a) Katô, H.; Taniguchi, M.; Katô, T. *Chem. Phys. Lett.* **1972**, *14*, 231–233. (b) Holt, S.; Dingle, R. *Acta Chem. Scand.* **1968**, *22*, 1091–1096. (c) Katô, H. *J. Chem. Phys.* **1973**, *59*, 1732–1737. (d) Hatfield, W. E. *Inorg. Chem.* **1964**, *3*, 605–606. (e) Drummond, J.; Wood, J. S. *Chem. Commun.* **1969**, 1373. (f) Zhang, Y.; Gebhard, M. S.; Solomon, E. I. *J. Am. Chem. Soc.* **1991**, *113*, 5162–5175. (g) Deaton, J. C.; Gebhard, M. S.; Solomon, E. I. *Inorg. Chem.* **1989**, *28*, 877–889.
(37) Creutz, C. *Prog. Inorg. Chem.* **1983**, *30*, 1–73.
(38) Westmoreland, T. D.; Wilcox, D. E.; Baldwin, M. J.; Mims, W. B.; Solomon, E. I. *J. Am. Chem. Soc.* **1989**, *111*, 6106–6123.
(39) Klotz, I. M.; Klotz, T. A.; Fiess, J. A. *Arch. Biochem. Biophys.* **1957**, *68*, 284–299.
(40) Buffer abbreviations used: Tris = tris(hydroxymethyl)aminomethane, MES = 2-*N*-morpholinoethanesulfonic acid, HEPES = *N*-(2-hydroxyethyl)piperazine-*N*′-2-ethanesulfonic acid, CHES = 2-(*N*-cyclohexylamino)-ethanesulfonic acid.
(41) For reasons that are unclear, occasionally the protein gave odd kinetics results, and the ϵ ratios of the UV–vis absorption peaks were not consistent with the published values. When this occurred the protein was crystallized by dialysis at 4 °C against a 15% ethanol/0.10 M Tris(SO$_4^{2-}$) pH 7.7 buffer. The crystals were collected by centrifugation, washed with the crystallization buffer, and finally dissolved in the desired buffer. In most cases this gave protein with ABS and kinetics behavior consistent with the literature. The crystallization step was usually not necessary, as the standard preparation gave sufficiently pure Hr.
(42) These buffers were chosen because they maintain their pH over a wide temperature range.[43]
(43) (a) Williams-Smith, D. L.; Bray, R. C.; Barber, M. J.; Tsopanakis, A. D.; Vincent, S. P. *Biochem. J.* **1977**, *167*, 593–600. (b) Orii, Y.; Morita, M. J. *J. Biochem.* **1977**, *81*, 163–168.
(44) The Na$_2$SO$_4$ stabilized the protein near its isoelectric point (pH = 7.6) and gave better glasses in the MCD experiments. Results at high and low Na$_2$SO$_4$ concentrations were identical.

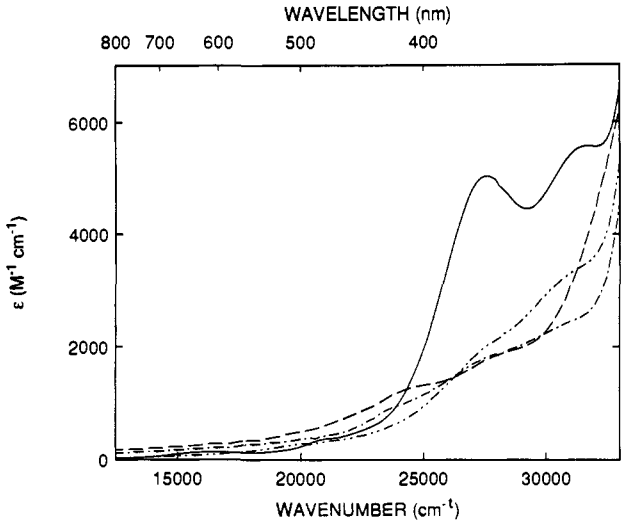

Figure 1. Absorbance spectrum of metF⁻ (—), $^1/_2$metF⁻ (-·-), $^1/_2$met$_r$ (– – – –) and $^1/_2$met$_o$ (--) in the charge-transfer region.

conversion to $^1/_2$metN_3^- (ϵ_{470nm} = 2400 M^{-1} cm^{-1}) with a small volume of 5.0 M NaN_3.[17d] This method indicated greater than 95% conversion to $^1/_2$met in all cases.

Protein samples for MCD were first converted to $^1/_2$met as described above and then made ~66% glycerol by volume by addition to anaerobic glycerol (for NIR MCD $C_3H_5(OD)_3$ was used). Depolarization of the MCD samples was checked using nickel tartrate,[7] which for all samples was less than ~12%. Analysis of the MCD samples for complete conversion to $^1/_2$met gave results similar to the ABS and CD samples.

Absorbance measurements from 300 to 820 nm were performed on an HP8452A spectrometer, with extension to 1800 nm on a Cary 17 instrument. CD and MCD spectra between 300 and 1100 nm were obtained on a JASCO J500C spectropolarimeter equipped with an Oxford SM4-6T magnet for MCD,[46] and spectra from 800 to 1800 nm were obtained on a JASCO J200D equipped with an Oxford SM4-7T magnet. All low-temperature MCD (LT MCD) spectra were recorded at 4.2 K and 5.0 T field. A Bruker ER 220D-SRC EPR equipped with an Air Products L2R-110 He cryostat was used to obtain the EPR spectra. The single-crystal spectra of metN_3^- were taken on a McPherson spectrometer; the instrument and experimental procedures have been described previously.[8]

The interconversion of $^1/_2$met$_r$ and $^1/_2$met$_o$ was studied by anaerobic reduction of metHr (~2–3 mM) at pH 7.0 by a 10-fold molar excess of $Na_2S_2O_4$. After mixing, the protein was immediately exposed to a stream of O_2 at 4 °C for 30 s with constant mixing. Conversion to $^1/_2$met$_r$ was confirmed by UV–vis ABS and quantitated as described above with similar results. The sample was divided and dialyzed aerobically against pH 6.0, 7.0, or 8.2 buffer with several buffer changes. After 24 h, the CD and EPR spectra of the samples were taken. The amount of $^1/_2$met, met, and oxy was quantitated by CD (500–1100 nm) by addition of a small volume of a concentrated Br^- solution (final [Br^-] = ~0.1 M). The CD spectra were fit to the known CD spectra of metBr⁻, oxy, and $^1/_2$metBr⁻.[8]

The kinetics of the interconversion of $^1/_2$met$_r$ and $^1/_2$met$_o$ at high and low pH with direct addition of redox agents was also examined. $^1/_2$Met samples were prepared by anaerobic addition of 1 equiv of redox agent to met or deoxy at pH 6.0 and 9.0 in a CD cell as described above. The time course of the reactions was monitored by CD at 1030 nm. When the CD signal showed minimal changes with time, the full CD and EPR spectra of the products were recorded.

Results

Charge-Transfer Region. Figure 1 shows the ABS spectra of metF⁻, $^1/_2$metF⁻, $^1/_2$met$_r$, and $^1/_2$met$_o$ in the region from 12 500 to 33 000 cm^{-1}. MetF⁻ shows two intense bands at 27 600 and 31 500 cm^{-1} with ϵ of 5000 and 5600 M^{-1} cm^{-1}, respectively.[8,14] These features are not present in the $^1/_2$met species in Figure 1, which show several shoulders in the region between ~20 000 and 33 000 cm^{-1}, with ϵ < 3000 M^{-1} cm^{-1}.

Table I

	exogenous ligand to Fe^{3+} LMCT obsd in I/2metL⁻	exogenous ligand to Fe^{3+} LMCT obsd in metL⁻
L⁻ =	energy (cm^{-1})	energy (cm^{-1})[7]
N_3^-	21 300[a,b]	21 500[d]
	29 100,[b] 20 200[c]	28 400[d]
	30 900[a]	
SCN^-	21 600[b]/21 400[a]	21 100[d]
	31 500[a]	30 700[d]
Br^-	23 400[c]	20 400[a]
	24 900[b]	24 400[c]
	27 100[c]	~28 500[c]
Cl^-	29 100[a]	28 100[c,e]
	30 500[c]	
CN^-	~25 000[b,f]	~25 100[c,e]
OCN^-	28 100[c]	28 300[b,c]

[a] From ABS at room temperature. [b] From MCD at 4.2 K. [c] From CD at room temperature. [d] From ⊥ polarized single-crystal ABS. [e] Inferred position.[7] [f] MCD at 4.2 K has increased intensity relative to 1/2metF⁻, but no obvious peak in this region.

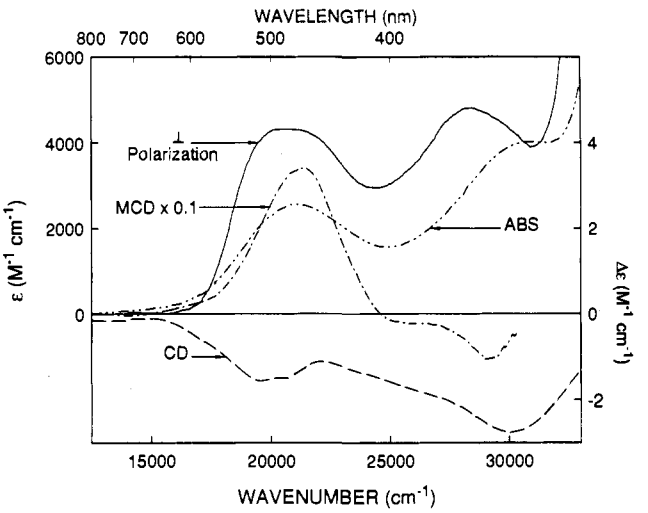

Figure 2. ABS (– – – –), LT MCD (-·-), CD (--) of $^1/_2$metN_3^- Hr in the charge-transfer region. Also shown is the ⊥ polarization of the single-crystal-polarized ABS spectrum of metN_3^- (—) in the same region.

A number of the $^1/_2$metL^- derivatives show additional transitions, assignable as exogenous ligand to Fe^{3+} LMCT transitions, in the 12 500–33 000-cm^{-1} region as given in Table I. These transitions are lowest in energy and most intense for L^- = N_3^- and SCN^-. ABS, CD, and LT MCD spectra in this region for $^1/_2$metN_3^- are shown in Figure 2. Also included in Figure 2 is the ⊥ polarization of the single-crystal-polarized ABS spectrum of metN_3^- which exhibits predominantly N_3^- to Fe^{3+} LMCT intensity.[8] The $^1/_2$metN_3^- ABS shows a peak at 21 300 cm^{-1} with an intense positive feature at the same energy in the LT MCD. The only other ABS feature is a peak at 30 900 cm^{-1}. The LT MCD has additional features at 26 100 and 29 100 cm^{-1}. The CD shows two negative peaks at 19 600 and 20 600 cm^{-1}, which are not apparent in the LT MCD or ABS (note the CD bands near 20 000 cm^{-1} do not peak at the same energy as the LT MCD or ABS spectra), and a more intense negative feature at 30 200 cm^{-1}. The 21 300-cm^{-1} band in the LT MCD and ABS is similar in energy to a band in the ⊥ polarized metN_3^- single-crystal ABS spectrum at 21 500 cm^{-1}, while the 30 000-cm^{-1} band is at higher energy relative to the 28 400 cm^{-1} transition in the ⊥ polarized metN_3^- single-crystal ABS spectrum.

Ligand Field Region. The CD, ABS, and LT MCD spectra for $^1/_2$metCl^- (which has no low-energy exogenous ligand LMCT

(45) It was found that addition of N_3^- to $^1/_2$met$_r$ at pH 6.00 gave relatively high concentrations of deoxyN_3^-, which was unacceptable for MCD, as the intense MCD transitions at ~10 000 cm^{-1} associated with deoxyN_3^- obscured those from $^1/_2$metN_3^-. At pH 7.00 formation of deoxyN_3^- was not significant, and therefore $^1/_2$metN_3^- was studied at this pH. All other $^1/_2$metL^- were studied at pH 6.00 as the MCD indicated that at pH 7.00 there was incomplete conversion from $^1/_2$met$_r$.

(46) Allendorf, M. A.; Spira, D. J.; Solomon, E. I. *Proc. Natl. Acad. Sci. U.S.A.* **1985**, *82*, 3063–3067.

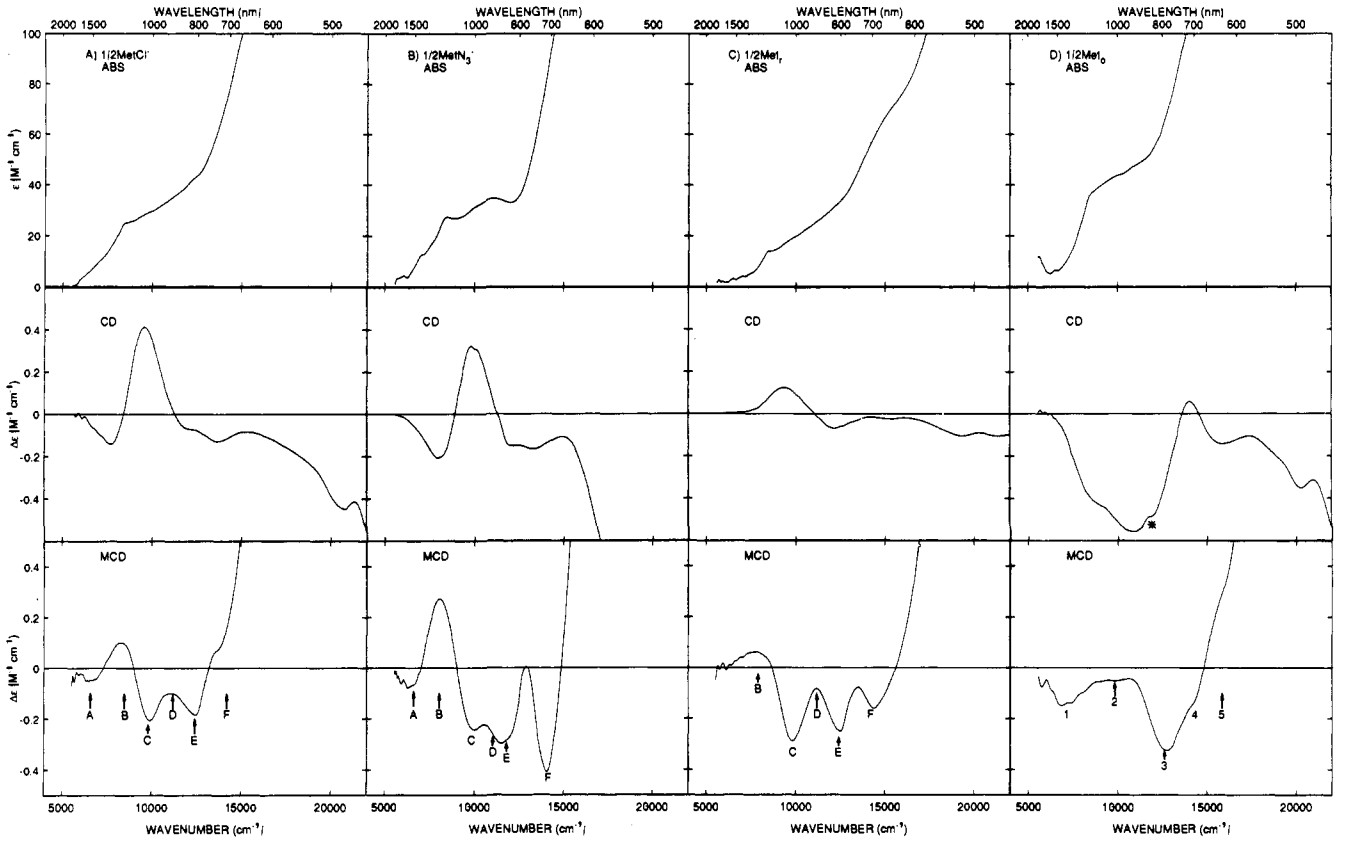

Figure 3. ABS, CD, and LT MCD spectra (from top to bottom) of (A) $^1/_2$metCl$^-$, (B) $^1/_2$metN$_3^-$, (C) $^1/_2$met$_r$, and (D) $^1/_2$met$_o$ in the ligand field region. The * in the CD spectrum of $^1/_2$met$_o$ indicates an instrumental artifact.

Table II. Gaussian-Resolved Bands in the Ligand Field Region of 1/2MetHr[a]

derivative	A (IT)[b]	B (IT)	C (Fe^{2+})	D (Fe^{3+})	E (Fe^{2+})	F (Fe^{3+})
1/2metN$_3^-$	6625 (−0.25)	8051 (+0.29)	9840 (−0.24)	11050 (−0.16)	11800 (−0.24)	14140 (−0.44)
1/2metOCN$^-$	7120 (−0.11)	9290 (+0.068)	9740 (−0.21)	11000 (−0.01)	12000 (−0.23)	14500 (−0.14)
1/2metCl$^-$	6560 (−0.05)	8510 (−0.12)	9790 (−0.22)	11200 (−0.07)	12400 (−0.21)	14200 (−.089)
1/2metSCN$^-$	7200 (−0.25)	8980 (+0.15)	9770 (−0.22)	10900 (−0.10)	11800 (−0.22)	14100 (−0.14)
1/2metCN$^-$	6780 (+0.11)	8510 (−0.13)	9710 (−0.23)	10800 (−0.04)	12100 (−0.18)	13700 (−0.13)
1/2met$_r$		7900 (+0.066)	9810 (−0.30)	11200 (−0.05)	12400 (−0.25)	14400 (−0.16)

derivative	1 (Fe^{2+})	2 (IT)	3 (Fe^{2+})	4 (Fe^{3+})	5 (Fe^{3+})
1/2met$_o$	7100 (−0.14)	9800 (−0.048)	12600 (−0.32)	14300 (−0.12)	15800 (+0.25)

[a] Table entries are band energies in cm^{-1} determined from the fit of the LT MCD at 4.2 K and 5.0 T field and are followed in parentheses by $\Delta\epsilon$ (in M^{-1} cm^{-1}) at this temperature and field. [b] Estimated error for the energies of bands A–C is ±100 cm^{-1}, and for bands D–F the error is ±200 cm^{-1}.

transition below 29 000 cm^{-1}), $^1/_2$metN$_3^-$, $^1/_2$met$_r$, and $^1/_2$met$_o$ in the 5000–20 000-cm^{-1} spectral region are shown in Figure 3. The ABS intensity of $^1/_2$metCl$^-$ (Figure 3A, top) and $^1/_2$metN$_3^-$ (Figure 3B, top) is small at energies less than ~6000 cm^{-1}.[47] To higher energy the intensity rises to a shoulder located at 8800 cm^{-1} in $^1/_2$metN$_3^-$ and at 9000 cm^{-1} in $^1/_2$metCl$^-$. $^1/_2$MetN$_3^-$ shows a more intense peak at 11 600 cm^{-1}, while this region in $^1/_2$metCl$^-$ is broad and featureless. The ABS spectrum of $^1/_2$met$_r$ (Figure 3C, top) is similar to that of the $^1/_2$metL$^-$, although slightly less intense, with shoulders at 9000 and 14 900 cm^{-1}. The ABS spectrum of $^1/_2$met$_o$ (Figure 3D, top) has a broad shoulder at 10 000 cm^{-1}, which is ~1.5–2 times more intense than the other $^1/_2$met species. Qualitatively, the CD and LT MCD spectra for $^1/_2$metN$_3^-$, $^1/_2$metCl$^-$, and $^1/_2$met$_r$ are quite similar, while $^1/_2$met$_o$ is very different both in terms of spectral shapes, peak positions, and peak intensities.

To aid in the analysis of the ligand field region the ABS, CD, and LT MCD spectra of the $^1/_2$metL$^-$s (Figures 3A,B and 4), $^1/_2$met$_r$ (Figure 3C), and $^1/_2$met$_o$ (Figure 3D) were simultaneously fit to a set of Gaussian bands.[48] Six bands were required to fit $^1/_2$metL$^-$, and five bands were required for $^1/_2$met$_r$ and $^1/_2$met$_o$. Because of the similarity between $^1/_2$metL$^-$ and $^1/_2$met$_r$ the bands are labeled A–F for these $^1/_2$met derivatives, while the bands are labeled 1–5 for $^1/_2$met$_o$. The energy and intensity of the resolved bands are given in Table II, and the energy of each band is indicated in the LT MCD spectra at the bottom of Figures 3 and 4B. Plots showing the full Gaussian-resolved spectra of each $^1/_2$met are given in the supplementary material (Figures S1–S4).

The CD and LT MCD reveal that a number of transitions are present in the 5000–20 000-cm^{-1} region. The first CD feature in $^1/_2$metCl$^-$ (Figure 3A, middle) and $^1/_2$metN$_3^-$ (Figure 3B, middle) is a negative band at ~8000 cm^{-1}, which the LT MCD (Figure 3A,B, bottom) shows to be comprised of two bands (bands A and B). The ~8000-cm^{-1} band is present in all $^1/_2$metL$^-$, as shown in Figure 4A. In the LT MCD (Figure 4B and Table II), bands A and B show large perturbations in terms of peak positions, signs, and intensities with changes in the exogenous ligand. The CD

(47) The weak ($\epsilon \approx 4$ M^{-1} cm^{-1}) feature at 6010 cm^{-1} in the $^1/_2$metN$_3^-$ ABS is a protein overtone that was not completely canceled by the baseline subtraction in this sample.

(48) Each spectroscopic method has different selection rules, and although transitions can have different intensities, and in the case of CD and LT MCD different signs, the energies and bandwidths will be independent of the spectroscopic probe. However, because the LT MCD was carried out at 4.2 K, bandwidths will be substantially narrower and band energies may shift slightly relative to the CD and ABS which were obtained at 300 K. These effects were taken into account in each fit.

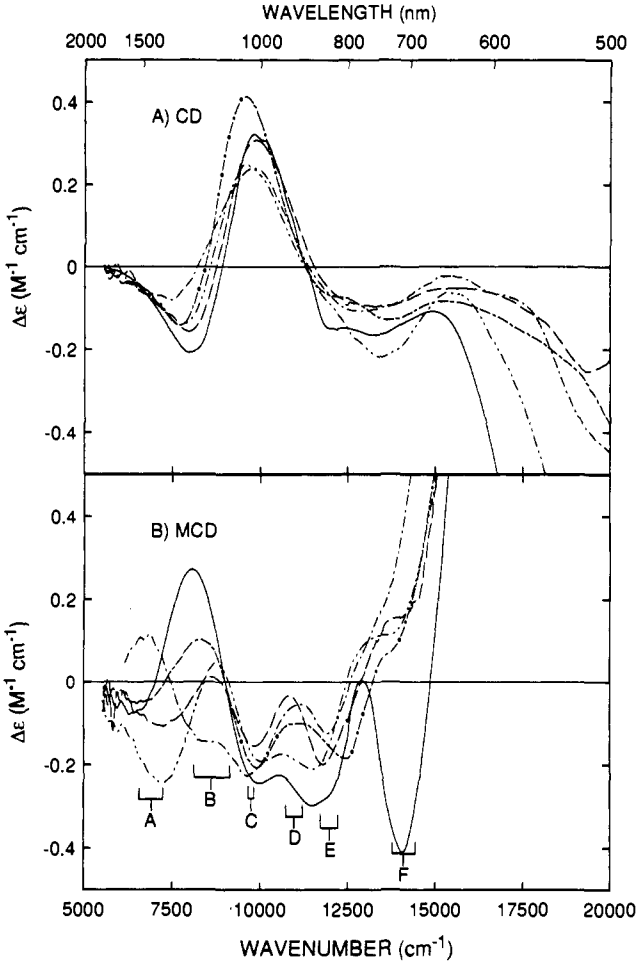

Figure 4. (A) CD spectra and (B) MCD spectra of $^1/_2$metL$^-$ in the ligand field region: L$^-$ = N_3^- (—), Cl^- (— — —), OCN^- (- -), SCN^- (— - — -), CN^- (- · -).

spectrum of $^1/_2$metCl$^-$ and $^1/_2$metN_3^- shows a positive feature of ~9800 cm^{-1} with a negative LT MCD band (band C) at the same energy. Band C is perturbed only slightly by changes in the exogenous ligand as shown in Figure 4B and Table II. The 9800-cm^{-1} positive CD feature tails into a broad negative feature with a shoulder at 12 000 cm^{-1} (12 400 cm^{-1} in $^1/_2$metCl$^-$) and a peak at 13 200 cm^{-1} in $^1/_2$metN_3^- (13 700 cm^{-1} in $^1/_2$metCl$^-$). The LT MCD clearly shows two negative features in this region at 12 100 (band E) and 14 100 cm^{-1} (band F) in $^1/_2$metN_3^-. $^1/_2$MetCl$^-$ has a negative LT MCD feature at 12 400 (band E) and a weak positive feature at 14 600 cm^{-1} which is resolved (supplementary material Figure S1C) as a negative band at 14 200 cm^{-1} (band F) on a higher energy positive feature. In addition, the low-temperature CD of the $^1/_2$metL$^-$ show a weak positive shoulder at ~11 000 cm^{-1}, which is also required in the Gaussian resolution of the LT MCD of all $^1/_2$metL$^-$ (band D).[49] As band D is overlapping with bands C and E its energy is not precisely known; however, its intensity is enhanced in $^1/_2$metN_3^- and $^1/_2$metSCN$^-$ relative to $^1/_2$metCl$^-$ (Table II and Figure 4B). The energies of bands E and F are perturbed by changes in exogenous ligand (Figure 4B and Table II), although the error associated with the energy of bands E and F in the fit is the same as the observed changes in band E. The intensity of band E is not perturbed by changes in exogenous ligand (Figure 4B and Table II), while the intensity of band F is perturbed, especially in $^1/_2$metN_3^-.

The CD spectrum of $^1/_2$met$_r$ (Figure 3C, middle) has no obvious band at ~8000 cm^{-1}, but the LT MCD (Figure 3C, bottom) has a weak positive feature at 7800 cm^{-1} (band B). The $^1/_2$met$_r$ CD has a positive feature at 9400 cm^{-1}, which is ~400 cm^{-1} lower in energy than the LT MCD peak at 9800 cm^{-1} (band C), and a negative feature at 12 200 cm^{-1}, with a corresponding negative LT MCD feature (band E) at 12 400 cm^{-1}. An additional band is observed in the low-temperature CD of $^1/_2$met$_r$ at ~11 000 cm^{-1} (Figure S5A in the supplementary material), which is also required in the Gaussian analysis (band D). $^1/_2$Met$_r$ also has a weak negative CD feature at 15 300 cm^{-1} and a well-resolved LT MCD band at 14 500 cm^{-1} (band F in Figure 3C, bottom).

$^1/_2$Met$_o$ exhibits an increase in its ABS intensity below 6000 cm^{-1} (Figure 3D, top) observed in the difference between the spectra of $^1/_2$met$_o$ and $^1/_2$metCl$^-$. However, neither the CD nor the LT MCD spectra show any evidence for a band at lowest energy. Thus the ABS intensity below 6000 cm^{-1}, also reported in our preliminary communication,[28] does not appear to be inherent to the $^1/_2$met$_o$ site.[50] The LT MCD (Figure 3D, bottom) has a negative feature at 7100 cm^{-1} (band 1). This LT MCD data provide a clear definition of the band position and shape without the complications due to baseline subtraction inherent to the NIR ABS at lowest energy. The $^1/_2$met$_o$ CD (Figure 3D, middle) has a shoulder at 9000 cm^{-1} off a broad, intense feature which peaks at 10 900 cm^{-1}. In the low-temperature CD (Figure S5B in the supplementary material), the 10 900-cm^{-1} band shows a large decrease in intensity, while band 1 does not. In addition, the 10 900-cm^{-1} CD peak has only weak LT MCD intensity (the Gaussian analysis requires a weak negative band (band 2) at 9800 cm^{-1}). The most intense LT MCD band in $^1/_2$met$_o$ is the negative band at 12 600 cm^{-1} (band 3). In addition, the CD and LT MCD show weaker features at 14 200 cm^{-1} (band 4) and 16 000 cm^{-1} (band 5).

All $^1/_2$met species have two additional CD features at ~18 000 and ~21 000 cm^{-1}, shown in Figure S6A of the supplementary material (also Figures 2 and 3C,D, middle). In all $^1/_2$metL$^-$ and $^1/_2$met$_r$ where this region is not obscured by low-energy exogenous LMCT (as for L$^-$ = N_3^-, SCN^-), the corresponding LT MCD spectra (Figure S6B) show a broad peak at ~18 000 cm^{-1}, whose energy is perturbed by changes in the exogenous ligand, and a peak at 21 400 cm^{-1}, which is relatively insensitive to changes in exogenous ligand.

Ground State. The 5.3 K EPR spectra of $^1/_2$metN_3^-, $^1/_2$met$_r$, and $^1/_2$met$_o$ are shown in Figure 5, and the dimer g values are given in Table III (those for other $^1/_2$metL$^-$ are shown in Table S1 of the supplementary material). The spectra and dimer g values are similar to those previously reported.[20a] The EPR spectra of $^1/_2$met$_r$ and $^1/_2$metL$^-$ are very similar (rhombic, $g_{\perp,av} > g_\parallel$), but the spectrum of $^1/_2$met$_o$ is quite different (axial, $g_\parallel > g_\perp$).

Variable field MCD (VH MCD) at low temperature (< ~2 K) provides an additional means of probing the lowest sublevel of the ground state and is an important first step in the analysis of the VT MCD data. The low-temperature variable field MCD data for $^1/_2$metN_3^- and $^1/_2$met$_o$ are given in Figure 6; neither show complete saturation of the MCD signal up to 5.0 T due to the

Table III. MCD and EPR Parameters for the Ground and Lowest Excited States of 1/2MetN_3^-, 1/2Met$_r$, and 1/2Met$_o$

	1/2metN_3^-	1/2met$_r$	1/2met$_o$
dimer, g_x, g_y	1.90, 1.82	1.94, 1.86	1.71, 1.71
dimer g_z	1.50	1.65	1.95
$B_0 \times 10^{-2}$	4.28 ± 0.02		1.1 ± 0.3
$m_z/m_{x,y}$	0.00 ± 0.04		0.00 ± 0.01
$B \times 10^{-2}$	4.23 ± 0.02	7.03 ± 0.02	0.00 ± 0.04
C_0	+1.12 ± 0.01	+1.09 ± 0.01	−1.12 ± 0.01
C_1	−0.7 ± 0.1	−1.8 ± 0.1	−2.9 ± 0.1
W_1 (cm^{-1})	18. ± 2	21. ± 2	18. ± 2
C_2			+3.0 ± 0.5
W_2 (cm^{-1})			33. ± 5

(49) The 4.2 K CD spectrum of $^1/_2$metCl$^-$ in Figure 11B (vide infra) clearly shows the weak shoulder at ~11 000 cm^{-1}.

(50) While this band could be due to residual deoxy, it appears to be eliminated upon addition of Cl^- (which does not bind to deoxy)[7] and is not present in the CD. We have observed that exposure of $^1/_2$met$_o$ samples to O_2 results in formation of a precipitate and some denaturation of the protein. This could result in a rising ABS baseline at low energy relative to the other $^1/_2$mets which do not show this effect.

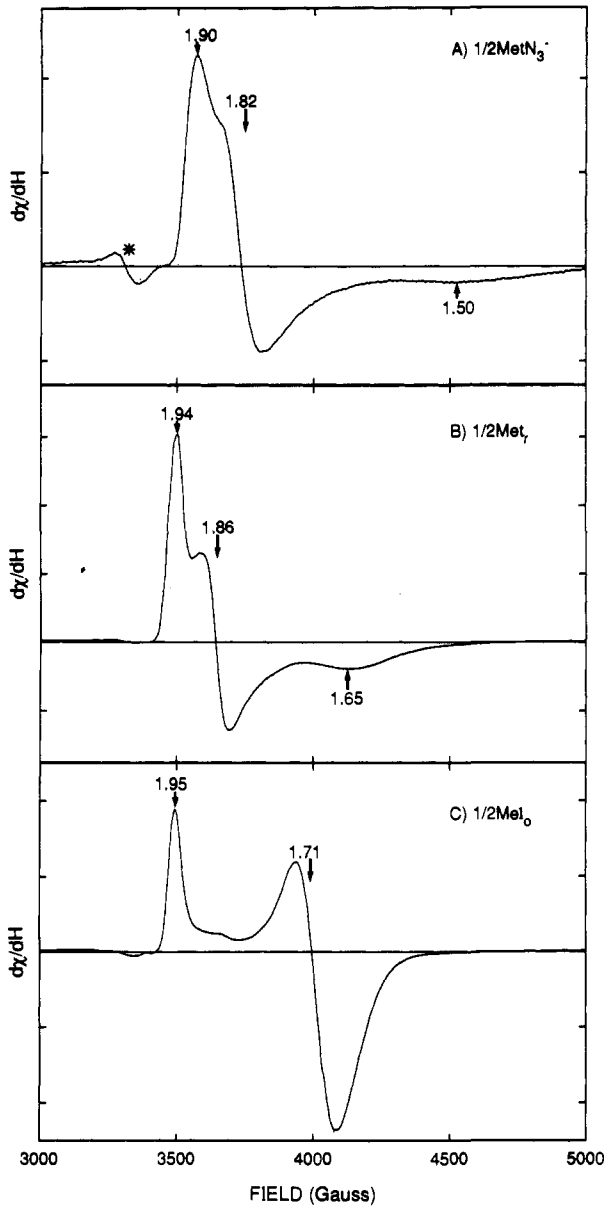

Figure 5. EPR spectra of (A) $^1/_2$metN$_3^-$ (pH 7.0), (B) $^1/_2$met$_r$ (pH 7.0) and (C) $^1/_2$met$_o$ (pH 6.0). EPR spectra were obtained at 5.3 K in an X band cavity with 2 mW microwave power and a modulation of 16 G. All samples were prepared as described in the Experimental Section and frozen in EPR tubes within ~40 s of preparation. The feature (marked by *) in the $^1/_2$metN$_3^-$ spectrum is an adventitious radical. The positions of the dimer g values given in Table III are indicated.

fairly low g values of the site. The orientation averaged expression for MCD intensity for a Kramers doublet is given in eq 1[51]

$$\Delta\epsilon = Km_{x,y}^2\left\{\int_0^{\pi/2}\frac{\cos^2\Theta\sin\Theta}{\Gamma}g_\parallel\tanh\left[\frac{\Gamma\beta H}{2k_bT}\right]d\Theta - \sqrt{2}\frac{m_z}{m_{x,y}}\int_0^{\pi/2}\frac{\sin^3\Theta}{\Gamma}g_\perp\tanh\left[\frac{\Gamma\beta H}{2k_bT}\right]d\Theta\right\} + B_oH \quad (1)$$

$$\text{where} \quad \Gamma = (g_\parallel^2\cos^2\Theta + g_\perp^2\sin^2\Theta)^{1/2}$$

where $\Delta\epsilon$ is the MCD intensity, K is a collection of physical constants, H is the applied magnetic field, k_b is the Boltzmann constant, the g values are those of the dimer, m_z and $m_{x,y}$ are, respectively, the transition dipole moments for the z- and x,y-polarized transitions,[52] and the parameter B_0 accounts for field

(51) Bennett, D. E.; Johnson, M. K. *Biochim. Biophys. Acta* **1987**, *911*, 71–80.

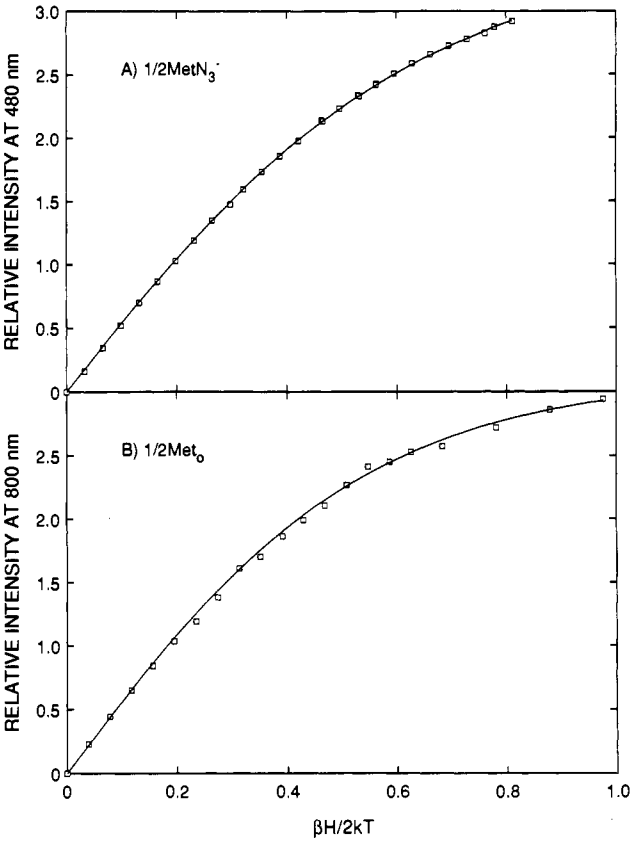

Figure 6. VH MCD (0.0–5.0 T) for (A) $^1/_2$metN$_3^-$ at 480 nm and 2.03 K and (B) $^1/_2$met$_o$ at 800 nm and 1.73 K. The intensities are normalized such that the $^1/_2$metN$_3^-$ intensity at 2.03 K and 1.0 T had an intensity of 1.0; the $^1/_2$met$_o$ intensity was normalized to 2.0 at 1.73 K and 2.0 T.

induced mixing of the ground state with high-lying excited states (MCD B-term).[53,54] The VH MCD data in Figure 6 were fit to eq 1 with a simplex routine[55] using the dimer g values given in Table III,[56] with the polarization ratio ($m_z/m_{x,y}$) and B_0 as adjustable parameters. The best fit polarization ratio and B_0 for $^1/_2$metN$_3^-$ and $^1/_2$met$_o$ are given in Table III.

The VT MCD data for $^1/_2$metN$_3^-$, $^1/_2$met$_r$, and $^1/_2$met$_o$ are shown in Figure 7. A full fit of the VT MCD data would require a Boltzmann population over a set of levels where the MCD intensity of each level would be given by an equation similar to eq 1; however, a number of simplifications can be made. The small polarization ratio ($\approx 10^{-2}$) obtained above indicates that the bands are essentially x,y-polarized; therefore, contributions from the second integral as well as B-terms arising from field-induced mixing of the $S_{tot} = {}^1/_2$ ground state with the $S_{tot} = {}^3/_2$ excited state are negligible. In this limit at nonsaturating fields a Boltzmann population over a series of levels with MCD intensity of each given by the first integral in eq 1 can be replaced by eq 2.[57] In eq 2, I is the experimental MCD intensity, C_i ($i = 0, 1, 2$) is the MCD C-term intensity parameter of the ith doublet, W_i

$$I = \sum_i\left(\frac{C_i}{k_bT}\alpha_i + B\right)H \quad (2)$$

$$\text{where} \quad \alpha_i = e^{-W_i/k_bT}/\sum_j e^{-W_j/k_bT}$$

is the energy of the ith doublet ($W_0 \equiv 0.0$), the parameter B again

(52) Note the term ($Km_{x,y}^2$) in eq 1 is a scaling factor and does not effect the overall saturation behavior.

(53) Equation 1 cannot be evaluated in a closed form and so was evaluated numerically by the method of Gaussian quadratures.[54]

(54) Press, W. H.; Flannery, B. P.; Teukolsky, S. A.; Vetterling, W. T. *Numerical Recipes*; Cambridge Press: 1988; pp 121–126.

(55) (a) O'Neill, R. *J. R. Statist. Soc. C* **1971**, *20*, 338–345. (b) Nelder, J. A.; Mead, R. *Computer J.* **1965**, *7*, 308–313.

(56) The dimer g_x and g_y given in Table II were averaged to give $g_\perp$.

(57) Browett, W. R.; Fucaloro, A. F.; Morgan, T. V.; Stephens, P. J. *J. Am. Chem. Soc.* **1983**, *105*, 1868–1872.

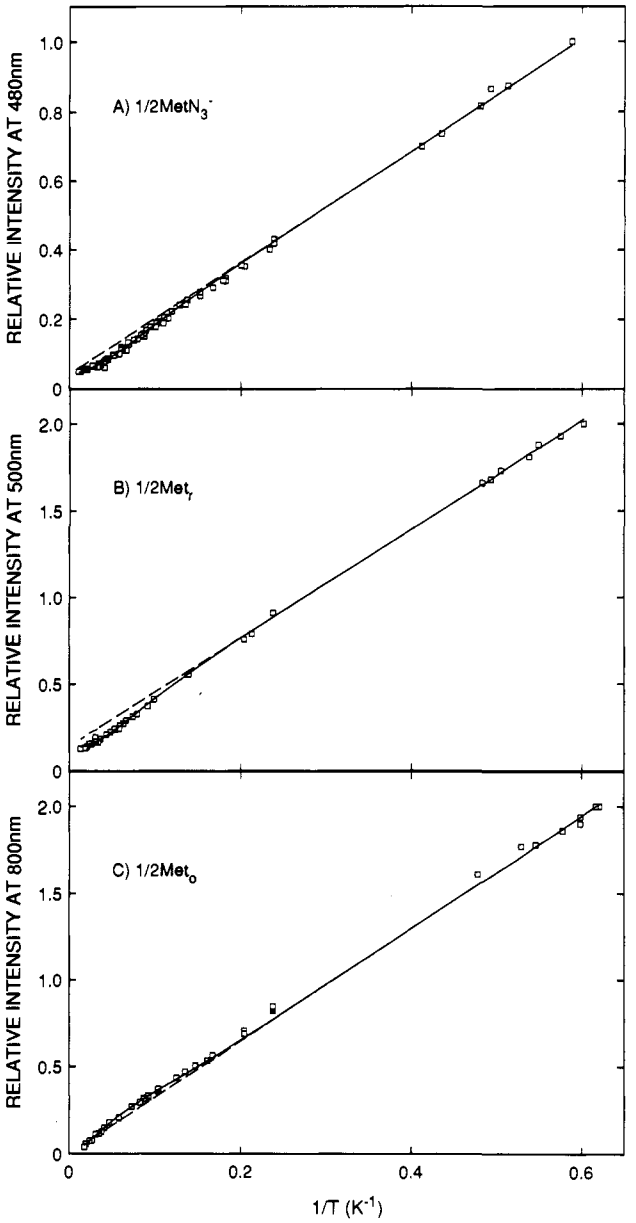

Figure 7. VT MCD data for (A) $^1/_2$metN$_3^-$ at 480 nm, 1.0 T field, (B) $^1/_2$met$_r$ at 500 nm, 2.0 T field, and (C) $^1/_2$met$_o$ at 800 nm, 2.0 T field. The data were normalized such that the lowest temperature point had an intensity of 2.0 for $^1/_2$met$_r$ and $^1/_2$met$_o$ and 1.0 for $^1/_2$metN$_3^-$. The Curie law behavior (--) is that predicted by the low-temperature data for an isolated Kramers doublet. The fit of the VT MCD data (—) is for the parameters shown in Table III and was obtained as described in the text.

accounts for field-induced mixing of the ground state and higher lying excited states, and k_b is Boltzmann's constant. The VT MCD data in Figure 7 were fit to eq 2,[55] with C_i, W_i, and B as adjustable parameters.[58] One excited state was necessary to obtain a good fit of the $^1/_2$met$_r$ and $^1/_2$metN$_3^-$ data, but two states were required for $^1/_2$met$_o$. The parameters of the best fit of each $^1/_2$met are given in Table III. Note that in Table III the B-term intensity found from the variable field MCD data with eq 1 (B_0) and that found from the VT MCD using eq 2 (B) analysis are in good agreement.

pH Dependence. Figure 8 shows the EPR of the $^1/_2$met derivatives obtained by reduction at pH 7.0, followed by aerobic dialysis into different pH buffers. The EPR spectra have been normalized to the concentration of $^1/_2$met found from the CD (Figure S6) and to the instrument gain. The EPR contains an adventitious radical at g = 2.00 (marked by a^* in Figure 8). The concentrations of $^1/_2$met, met, and oxy found at each pH are presented in Table S2 of the supplementary material. At pH 6.0 (Figure 8) the EPR spectrum of the product is axial with g = 1.94 and g = 1.70. The EPR spectrum of the pH 7.0 product shows an increase in the feature at g = ~1.94, while the intensity of the feature at g = 1.70 has decreased relative to pH 6.0, and a new feature has appeared at g = 1.86. At pH 8.2 the resonances at g = 1.94 and 1.86 have increased relative to pH 7, and the resonance at g = 1.70 has decreased.[59] No other resonances are observed at pH 8.2.

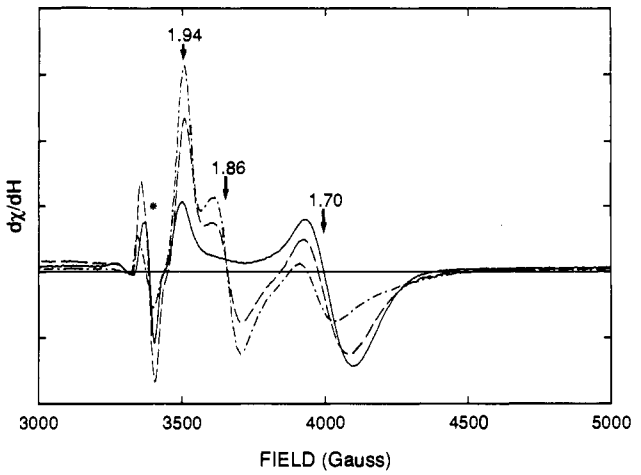

Figure 8. EPR spectra of the $^1/_2$met product obtained by reduction of met at pH 7.0 followed by dialysis into different pH buffers. Data are for pH 6.0 (—), pH 7.0 (--), and pH 8.2 (— — —). The instrument settings were the same as those given in Figure 5. The signal at g = 2.00 (marked by *) is an adventitious radical.

The EPR spectra (the CD spectra and kinetic traces are shown in Figures S8–S11 of the supplementary material) of the $^1/_2$met derivatives obtained by direct oxidation of deoxy and reduction of met at pH 6.0 and pH 9.0 are shown in Figure 9. The product of met reduction and deoxy oxidation at pH 6.0 have very similar EPR spectra with features at g values of 1.94 and 1.70. In addition, the EPR of the reduction product shows a weaker feature at g = 1.89 from residual $^1/_2$met$_r$ as the reaction was not allowed to go to completion. At pH 9.0 the metOH$^-$ reduction and deoxy oxidation both give a product whose EPR spectrum has features at g = 1.95, 1.86, and 1.68.

Spectral Assignments and Analysis

Charge-Transfer Region. The intense bands observed at 27 600 and 31 500 cm^{-1} in the ABS spectrum of metF$^-$ (Figure 1) have been assigned as oxo to Fe^{3+} LMCT transitions.[8] These bands are not present in the ABS spectrum of $^1/_2$metF$^-$ (Figure 1) indicating that the oxo bridge present in metF$^-$ has been eliminated or greatly perturbed in $^1/_2$metF$^-$. This is consistent with previous proposals that the oxo bridge is converted to a OH$^-$ bridge in $^1/_2$met.[19,28,29] As the exogenous F$^-$ has no LMCT transitions with Fe^{3+} below 35 000 cm^{-1},[8,60] the $^1/_2$metF$^-$ ABS spectrum in this region must reflect endogenous ligand to Fe^{3+} LMCT. The similarity of the ABS intensity of $^1/_2$met$_r$ and $^1/_2$met$_o$ to $^1/_2$metF$^-$ (Figure 1) indicates that the oxo bridge is similarly perturbed and furthermore that these features are endogenous ligand to Fe^{3+} LMCT. Transitions at this energy and intensity are consistent with the endogenous ligand to Fe^{3+} LMCT observed at 28 600 cm^{-1} in the mononuclear non-heme iron protein Fe^{3+}SOD.[61]

(58) In the fit of the VT MCD data each point was weighted by the reciprocal of the uncertainty in the temperature. In general, the measured error in the temperature is as follows: for $T \leq 2.2$ K the error is ±0.01 K; for $10 \leq T \leq 4.2$ the error is ±0.1–0.3 K, and for $T \geq 10$ K the error is ±0.1 K.

(59) The pH 8.2 EPR spectrum appears to have some residual amount of $^1/_2$met$_o$ present. This may be due in part to the temperature dependence of the equilibrium between $^1/_2$met$_r$ and $^1/_2$met$_o$ as well as the pH of the solution changing as the temperature is changed.

(60) Lever, A. B. P. *Inorganic Electronic Spectroscopy*, 2nd ed.; Elsevier: 1984; pp 218–258.

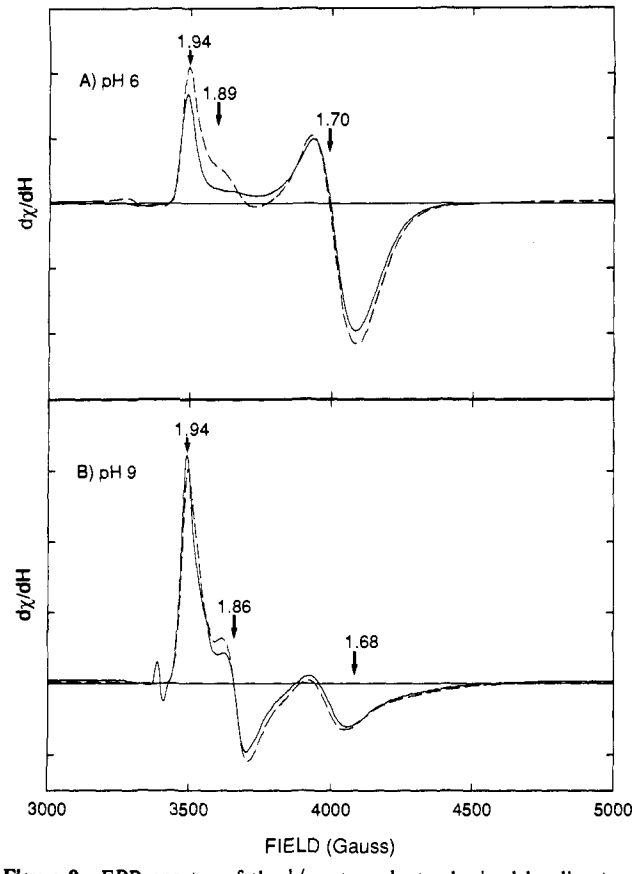

Figure 9. EPR spectra of the $^1/_2$met products obtained by direct reduction (———) or oxidation (—) at (A) pH 6.0 and (B) pH 9.0.

X-ray crystallography has shown that the Fe^{3+} in Fe^{3+}SOD has a ligand set similar to that of metHr (histidine and carboxylate coordination).[62]

MetL$^-$Hr crystallizes such that the ⊥-polarized single-crystal ABS spectrum of metL$^-$ will be a predominantly exogenous ligand to Fe^{3+} LMCT, while the ∥ polarization will be oxo to Fe^{3+} LMCT.[8,12j,63] The ABS spectrum of $^1/_2$metN_3^- in the charge-transfer region (Figure 2) is similar to the ⊥-polarized ABS spectrum of metN_3^-, indicating that the $^1/_2$metN_3^-, spectrum is dominated by N_3^- to Fe^{3+} LMCT. Other $^1/_2$metL$^-$ have transitions at energies similar to the exogenous ligand to Fe^{3+} LMCT in metL$^-$ (Table I); therefore, these $^1/_2$metL$^-$ transitions are assigned as exogenous ligand LMCT. The presence of exogenous ligand to Fe^{3+} LMCT in the $^1/_2$metL$^-$s demonstrates that the exogenous ligand is bound to the Fe^{3+} in all $^1/_2$metL$^-$.

The LMCT of $^1/_2$metN_3^- does differ, however, from the LMCT of metN_3^- in two ways: the band at 28 400 cm^{-1} in the ⊥-polarized single-crystal ABS of metN_3^- shifts to 30 000 cm^{-1} in $^1/_2$metN_3^-, and the shape of the band at 21 500 cm^{-1} changes, but the energy does not on going from metN_3^- to $^1/_2$metN_3^-. The ⊥-polarized single-crystal ABS spectrum of metN_3^- was fit to two pairs of bands centered at 21 500 and 28 400 cm^{-1}, with an intraset splitting of 2500 cm^{-1} and an interset splitting of 8000 cm^{-1}.[8] These data are not consistent with a linear N_3^-–Fe^{3+} bonding mode as in Figure 10A, indicating that the N_3^- is undergoing an additional strong interaction, and it was suggested the N_3^- might be protonated.[8] Protonation causes rehybridization of the azide valence orbitals, with respect to the Fe^{3+}, giving the energy level diagram in Figure 10B. The angle the N–H bond makes with the N_3–Fe plane (ϕ) determines the splitting of the N_3^- orbitals and the

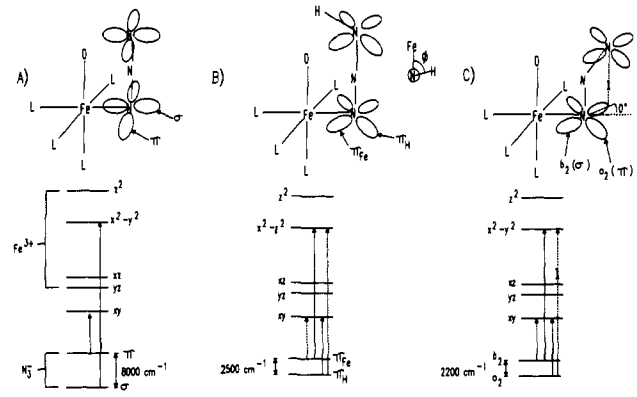

Figure 10. Energy level diagram for (A) a linear N_3^-, (B) for a protonated N_3^-, and (C) a bent N_3^- bound to a Fe^{3+}–oxo dimer. Weak transitions are indicated by dashed arrows. The energy level ordering for the Fe^{3+} d orbitals is that determined experimentally.[7]

intensities of the normally forbidden N_3^- to Fe^{3+} LMCT transitions shown as dashed arrows in Figure 10B. An alternative explanation for the N_3^- to Fe^{3+} LMCT spectrum in metN_3^- and $^1/_2$metN_3^-, not considered previously, relates to the fact that the azide binds bent (i.e., N–N–N angle less than 180°).

In the crystal structure of metN_3^-Hr, the N_3^- has an N–N–N angle of 160 (5)°, and the plane of the bent N_3^- makes an angle of 10 (5)° with the plane defined by the oxo-Fe-N_3^- (Figure 10C).[13,64] Distorting the N_3^- from linear $D_{\infty h}$ to bent C_{2v} symmetry splits the nonbonding $1\pi_g$ HOMO in $D_{\infty h}$ into levels with b_2 and a_2 symmetry in C_{2v}.[65] The b_2 orbital will be predominantly σ bonding, while the a_2 will be mostly π bonding to the Fe^{3+} (Figure 10C). A bent N_3^- bound to Fe^{3+} will have two allowed LMCT transitions: the N_3^- $a_2 \rightarrow Fe^{3+}$ d_{xy} and the more intense N_3^- $b_2 \rightarrow Fe^{3+}$ $d_{x^2-y^2}$ at higher energy (Figure 10C). Similar to the effects of protonation, the 10° rotation of the N_3^- mixes the N_3^- a_2 and b_2 levels giving intensity to the forbidden N_3^- $b_2 \rightarrow Fe^{3+}$ d_{xy} and N_3^- $a_2 \rightarrow Fe^{3+}$ $d_{x^2-y^2}$ transitions (dashed arrows in Figure 10C).

The changes in the N_3^- to Fe^{3+} LMCT spectrum on going from metN_3^- to $^1/_2$metN_3^- can be accounted for by either the protonated or bent N_3^- model. The band shape change of the band at 21 500 cm^{-1} requires a loss of intensity in the lower energy component of that pair. The protonated model requires a change in ϕ, while the bent model requires a decrease in the angle between the N_3^- plane and the Fe-oxo-N_3^- plane. In both there will be less overlap of the mostly σ bonding N_3^- orbital with the d_{xy} orbital on the Fe^{3+} and thus less intensity in the N_3^- (π_{Fe}/b_2) $\rightarrow Fe^{3+}$ d_{xy} transition. The ~2000-cm^{-1} shift of the 30 000-cm^{-1} band in $^1/_2$metN_3^- relative to metN_3^- reflects a change in the energy of the Fe^{3+} $d_{x^2-y^2}$ orbital, as the lower energy LMCT transitions have not changed. The crystal structure of metN_3^- shows the Fe^{3+} is shifted toward the oxo ligand to above the plane defined by the equatorial ligands.[13] In changing the bridge from oxo (metN_3^-) to hydroxo ($^1/_2$metN_3^-) the Fe^{3+} should shift into the equatorial plane because of the weaker Fe^{2+}–OH bond, causing the $d_{x^2-y^2}$ orbital, which is σ bonding to the equatorial ligands to increase in energy, while the d_{xy} orbital, which is π bonding to the equatorial ligands, will be less effected.[66]

Ligand Field Region. Bands A and B, the lowest energy bands in $^1/_2$metL$^-$ (Figures 3A,B and 4 and Table II), show large perturbations in terms of intensity, energy, and sign with changes in L$^-$ (Figure 4). These transitions must be associated with the Fe^{3+} as the presence of exogenous ligand to Fe^{3+} LMCT (vide supra) indicates that L$^-$ is bound to the Fe^{3+}. These bands are

(61) Dooley, D. M.; Karas, J. L.; Jones, T. F.; Cotê, C. E.; Smith, S. B. *Inorg. Chem.* **1986**, *25*, 4761–4766.
(62) Stallings, W. C.; Powers, T. B.; Pattridge, K. A.; Fee, J. A.; Ludwig, M. L. *Proc. Natl. Acad. Sci. U.S.A.* **1983**, *80*, 3884–3888.
(63) (a) Stenkamp, R. E.; Sieker, L. C.; Jensen, L. H. *Proc. Natl. Acad. Sci. U.S.A.* **1976**, *257*, 349–351. (b) Ward, K. B.; Hendrickson, W. A.; Klippenstein, G. L. *Nature* **1975**, *257*, 818–821.
(64) Protein structural parameters were obtained from the crystal structure information on file in the Brookhaven Protein Data Bank.[13]
(65) Walsh, A. D. *J. Chem. Soc.* **1953**, 2266–2288.
(66) Note the bent N_3^- model is not applicable to the peroxide bonding in oxyHr which has a qualitatively similar exogenous ligand to Fe^{3+} LMCT spectrum.[8] Therefore only the previous model analogous to Figure 10B of a hydroperoxide bound to an Fe^{3+} in oxyHr can account for its peroxide to Fe^{3+} LMCT spectrum.

lower in energy than is normally observed for high-spin Fe^{3+} ligand field bands.[36] In metL$^-$ the lowest energy Fe^{3+} ligand field transition ($^6A_1 \rightarrow {}^4T_1$) is observed at ~9700 cm^{-1} [8] and should shift to higher energy in $^1/_2$metL$^-$ if the strong field oxo ligand were replaced by the weaker field OH^- ligand. Therefore, bands A and B can be neither Fe^{2+} nor Fe^{3+} ligand field transitions and must correspond to IT transitions. Figure 11A shows that the ~8000-cm^{-1} CD band (arrow) associated with bands A and B in $^1/_2$metL$^-$ (Figure 3A,B) is not present in the CD of metL$^-$ and deoxyL$^-$, as expected for an IT band.[37] In addition, Cox has shown the intensity of the IT band in an antiferromagnetically coupled high-spin Fe^{2+}–Fe^{3+} system should decrease with decreasing temperature.[67] As shown in Figure 11B, the 8000-cm^{-1} CD band does indeed show a large loss of intensity relative to the ~9800-cm^{-1} band at low temperature. An IT transition should have no LT MCD intensity;[38] however, there are examples of mixed-valent systems where the IT band obtains some LT MCD intensity through spin-orbit coupling.[68]

Band C at ~9800 cm^{-1} in the $^1/_2$metL$^-$ LT MCD (Figure 4B) is insensitive to changes in the exogenous ligand and thus can be assigned as a Fe^{2+} ligand field band. As shown in Table II, band D (at ~11 000 cm^{-1}) gains intensity when L$^-$ has low-energy LMCT, as expected for a Fe^{3+} ligand field band, and based on its energy can be assigned as the $^6A_1 \rightarrow {}^4T_1$ Fe^{3+} ligand field band.[36] The ~2000-cm^{-1} shift to higher energy of this band in $^1/_2$metL$^-$ relative to metL$^-$ is consistent with the replacement of the oxo bridge in met with a OH^- bridge in $^1/_2$met. Band E at ~12 000 cm^{-1} (Figure 4B and Table II) is equal in LT MCD intensity to band C (Fe^{2+}), and its intensity is not perturbed when L$^-$ has low-energy LMCT transitions. Band E can therefore be assigned as a second Fe^{2+} ligand field band. The presence of two Fe^{2+} ligand field bands with $\Delta^5E \approx 2000$ cm^{-1} indicates the Fe^{2+} is six-coordinate.[33] Band F near 14 000 cm^{-1} in the LT MCD is partially obscured by a more intense higher energy band (Figure 4B), and so there is greater uncertainty in its position and intensity. However, it is clear that band F's intensity is greatly enhanced in $^1/_2$metN$_3^-$ and that it occurs at lowest energy in $^1/_2$metCN$^-$. Therefore, band F is assigned as a Fe^{3+} ligand field transition ($^6A_1 \rightarrow {}^4T_2$) shifted ~1000 cm^{-1} to higher energy relative to metL$^-$ by the weaker field OH^- bridging ligand. The presence of Fe^{3+} ligand field bands at ~11 000 and ~14 000 cm^{-1} indicates that the Fe^{3+} is six-coordinate.[36]

The observed ligand field bands in $^1/_2$met$_r$ (Figure 3C) can be assigned by comparison to the $^1/_2$metL$^-$ bands. Band B is assigned as IT; band A is not observed in $^1/_2$met$_r$ (Table II), although it may be very weak.[69] Note band B is much weaker in the LT MCD spectrum relative to band C (at 9800 cm^{-1}) in $^1/_2$met$_r$ as expected for an IT band.[70] Bands C and E are assigned as ligand field bands from a six-coordinate Fe^{2+}. Likewise, bands D and F are assigned as ligand field bands of a six-coordinate Fe^{3+}. The fact that $^1/_2$met$_r$ has a six-coordinate Fe^{2+} and a six-coordinate Fe^{3+} indicates the exogenous ligand of $^1/_2$metL$^-$ has been replaced by a water-derived exogenous ligand (i.e., H_2O or OH^-).

The intense feature at 10 900 cm^{-1} in the CD of $^1/_2$met$_o$ (Figure 3D, middle) has only weak LT MCD intensity (Figure 3D, bottom, band 2 at 9800 cm^{-1} in Table II), consistent with its assignment as an IT transition.[71] There is only one intense band in the LT MCD of $^1/_2$met$_o$, band 3 at 12 600 cm^{-1}. On the basis of its intensity compared to the ligand field transitions in $^1/_2$metL$^-$, band 3 in $^1/_2$met$_o$ is assigned as a Fe^{2+} ligand field band. It should be emphasized that the presence of a Fe^{2+} band at ~12 500 cm^{-1} and the lack of an equally intense band near 10 000 cm^{-1} indicates that the Fe^{2+} in $^1/_2$met$_o$ is five-coordinate.[33-35] A five-coordinate Fe^{2+} is expected to have a second ligand field transition ~5000–7000 cm^{-1} to lower energy. Band 1 is ~5500 cm^{-1} below band 3 in energy and can be reasonably assigned as the second Fe^{2+} ligand field band based on it being the second most intense band in the ligand field region of the LT MCD spectrum.[72,73] Fe^{2+} has no spin-allowed bands above 13 000 cm^{-1},[74] and therefore bands 4 and 5 in $^1/_2$met$_o$ at 14 300 and 15 800 cm^{-1} must be due to the Fe^{3+}.[75] The energies of these bands are consistent with two components of a low symmetry split $^6A_1 \rightarrow {}^4T_2$ ligand field transition of a six-coordinate Fe^{3+}.[76]

The $^1/_2$met LT MCD feature at 21 400 cm^{-1} (Figure S5B) and its corresponding CD feature (Figure S5A) must be due to the Fe^{3+}, as high-spin Fe^{2+} is not expected to have transitions at this energy.[74] The insensitivity of the 21 400-cm^{-1} band to changes at the Fe^{3+} center leads to its assignment as the ligand field independent $^6A_1 \rightarrow {}^4A_1, {}^4E$ d $\rightarrow$ d transition of the Fe^{3+}. The band at ~18 000 cm^{-1} may be a component of a Fe^{3+} ligand field band, although its sensitivity to changes in the exogenous ligand in the LT MCD and insensitivity in the CD make the assignment of this band uncertain.

IT Transition. The IT band can be used to gain further insight into the mixed-valent properties of the dimer using Hush's theory.[37,77] Although this treatment is quantitatively limited to the low delocalization limit,[38] its results will be qualitatively useful in comparing the $^1/_2$mets. Three parameters are obtained: α^2, the delocalization of the extra electron from the Fe^{2+} to the Fe^{3+}, ΔE_0, the energy difference between the potential well minima of the mixed-valent ground state ($|G\rangle$) and IT excited state ($|IT\rangle$), and χ, the nuclear reorganizational energy associated with the distortion (ΔQ) that occurs with the $|G\rangle \rightarrow |IT\rangle$ transition.[78] α^2,

Table IV. IT Band Spectral Parameters

	1/2MetCl$^-$	1/2MetN$_3^-$	1/2Met$_r$	1/2Met$_o$
ϵ_{max}[a] (M^{-1} cm^{-1})	14.0	13.0	7.0	43.0
$E_{1/2}$[a] (cm^{-1})	2900	2700	3200	3900
E_{max}[a] (cm^{-1})	7900	8200	8200	10400
α^2	2.0×10^{-4}	2.0×10^{-4}	1.0×10^{-4}	6.0×10^{-4}
χ[b] (cm^{-1})	2800 ± 600	2400 ± 500	3400 ± 700	5100 ± 1000
ΔE_0[b] (cm^{-1})	5100 ± 600	5800 ± 500	4800 ± 700	5300 ± 1000
H_{ab} (cm^{-1})	112.0	116.0	82.0	255.0
ΔG^* (kcal/mol)	5.4	5.5	5.7	6.8
k_{et} (s^{-1})	2.0×10^8	2.0×10^8	8.0×10^7	1.0×10^8

[a] These parameters were obtained from the simultaneous gaussian fit of the ABS, CD, and LT MCD data; see text for details. [b] The error bars represent the ranges in these parameters calculated using the range of ($\hbar\omega$), as described in the text.

(67) Cox, P. A. *Chem. Phys. Lett.* **1980**, *69*, 340–343.
(68) (a) Dubicki, L.; Ferguson, J. *Chem. Phys. Lett.* **1984**, *109*, 128–131. (b) Dubicki, L.; Ferguson, J.; Krausz, E. R.; Lay, P. A.; Maeder, M.; Taube, H. *J. Phys. Chem.* **1984**, *88*, 3940–3941. (c) Dubicki, L.; Krausz, E. *Inorg. Chem.* **1985**, *24*, 4661–4665. (d) Dubicki, L.; Ferguson, J.; Krausz, E. R. *J. Am. Chem. Soc.* **1985**, *107*, 179–182. (e) Dubicki, L.; Ferguson, J.; Krausz, E. R.; Lay, P. A.; Maeder, M.; Magnuson, R. H.; Taube, H. *J. Am. Chem. Soc.* **1985**, *107*, 2167–2171.
(69) Another possibility is that the negative feature is higher in energy than the positive band and thus obscured by band C at 9800 cm^{-1}. This would make $^1/_2$met$_r$ similar to $^1/_2$metCN$^-$ (Figure 4B).
(70) The 4.2 K CD (Figure S5A of the supplementary material) and the LT MCD of $^1/_2$met$_r$ both peak at 9800 cm^{-1}. This apparent ~400-cm^{-1} shift of the CD band to higher energy relative to the room-temperature spectrum and indicates that a band at lower energy cools out. The fact that the 7900-cm^{-1} band B in $^1/_2$met$_r$ shows this behavior is further evidence for its assignment as an IT band.
(71) This band also shows a decrease in its CD intensity upon cooling (see Figure S5B in the supplementary material).
(72) An alternate assignment of band 1 is that it is a second IT band, as in $^1/_2$metL$^-$ (Figures 3A,B and 4). However, band 1 shows a smaller loss of CD intensity relative to band 2 on going from room temperature to 4.2 K (see Figure S5B of the supplementary material), which is consistent with the ligand field assignment.
(73) Note that Δ^5E for the five-coordinate Fe^{2+} in $^1/_2$met$_o$ is 5500 cm^{-1}, while in deoxyHr Δ^5E is ≥7000 cm^{-1}. This indicates that there is some difference in the coordination geometries between the five-coordinate Fe^{2+} in deoxy and $^1/_2$met$_o$.
(74) Pollini, I.; Spinolo, G.; Benedek, G. *Phys. Rev. B* **1980**, *22*, 6369–6390.
(75) No transitions are observed in this region in either deoxy or deoxyN$_3^-$Hr (see Figure 11A).[7]
(76) An additional band, corresponding to the $^6A_1 \rightarrow {}^4T_1$ transition of a six-coordinate Fe^{3+}, could be included in the fit of the LT MCD data at ~11 000 cm^{-1}, but it was not required by the fit.
(77) (a) Hush, N. S. *Prog. Inorg. Chem.* **1967**, *8*, 391–444. (b) Hush, N. S. *Electrochim. Acta* **1968**, *13*, 1005–1023.
(78) The general expression for χ is $\chi = {}^1/_2(k_Q \Delta Q^2)$, k_Q being the force constant of the distorting mode Q.

ΔE_0, and χ are obtained from the spectroscopic parameters ϵ_{max} (extinction coefficient at the IT band maximum), $E_{1/2}$ (the IT band's full width at half maximum), and E_{max} (the energy of the IT band) as given below. These parameters are obtained from the fit of the room-temperature ABS spectrum of $^1/_2$metL$^-$ ($L^- = Cl^-, N_3^-$), $^1/_2$met$_r$, and $^1/_2$met$_o$ in conjunction with the room-temperature CD and the LT MCD spectra and are summarized in Table IV. Note that for $^1/_2$met$_o$ ϵ_{max} is about four times larger and E_{max} is about 1800 cm^{-1} higher in energy than the other $^1/_2$mets.

Equation 3 gives the expression for α^2, where R is the distance the electron is transferred in Å.[37,77] For $^1/_2$metN$_3^-$ it has been determined from EXAFS that the Fe–Fe distance is 3.46 Å,[30] which is used for R for all the $^1/_2$met derivatives. The calculated α^2 parameters for the four $^1/_2$met species are given in Table IV.

$$\alpha^2 = 4.24 \times 10^{-4}\epsilon_{max}E_{1/2}/(E_{max}R^2) \quad (3)$$

$^1/_2$Met$_r$ and $^1/_2$metL$^-$ have similar α^2, while $^1/_2$met$_o$ is approximately three times more delocalized than either $^1/_2$met$_r$ or $^1/_2$metL$^-$. The relationship between $E_{1/2}$ and χ is given by eq 4,[77] where $\hbar\omega$ is the energy of the principal distoring mode, T is the

$$(E_{1/2})^2 = 8\ \ln(2)\chi(\hbar\omega)\ \coth(\hbar\omega/2k_bT) \quad (4)$$

absolute temperature, and k_b is the Boltzmann constant. A range of reasonable $(\hbar\omega)_{eff}$ ($200 \le (\hbar\omega)_{eff} \le 600$ cm^{-1}) was considered to allow a comparison among the $^1/_2$mets, with the calculated ranges for χ at 300 K given in Table IV. χ for $^1/_2$met$_r$ and $^1/_2$metL$^-$ are again quite similar and indicate a similar distortion occurs for the IT transition. The value of χ for $^1/_2$met$_o$ is about twice that of the other $^1/_2$mets indicating a larger distortion occurs upon excitation to the IT excited state. This difference in χ between $^1/_2$met$_r$ and $^1/_2$met$_o$ is consistent with the analysis of the ligand field spectra which indicated that for $^1/_2$met$_r$ and $^1/_2$metL$^-$ both irons are six-coordinate, while in $^1/_2$met$_o$ the Fe^{2+} is five-coordinate and the Fe^{3+} is six-coordinate in the ground state. Therefore, for $^1/_2$met$_o$ transfer of the extra electron to the second iron in the IT transition should result in a state with a six-coordinate Fe^{2+} and five-coordinate Fe^{3+} which would be expected to be strongly distorted relative to the ground-state geometry. Having obtained values for χ from eq 4, eq 5 can be used to evaluate ΔE_0, the zero-point potential well energy separation.[77] Calculated values of ΔE_0 for all $^1/_2$mets are ~5000 cm^{-1} (Table IV). Finally, the IT band can be used to obtain the thermal electron-transfer rate constant k_{el} in the high-temperature limit (eq 6).[79] ΔG^* is the free energy of electron transfer and is given by the relationship $(E_{max}/4) - H_{ab}$,[37] where the resonance energy matrix element $H_{ab} = \alpha E_{max}$.[80] Calculated values of H_{ab}, ΔG^*, and k_{et} for $^1/_2$met$_r$, $^1/_2$met$_o$, and $^1/_2$metL$^-$ are given in Table IV. As expected given the similarity in their IT band spectral parameters, H_{ab} and ΔG^* for $^1/_2$met$_r$ and the $^1/_2$metL$^-$ are similar, and all the $^1/_2$met species are found to have k_{et} on the order of 10^8 s^{-1}.

$$k_{et} = \frac{2\pi^{3/2}H_{ab}^2}{h}(k_bTE_{max})^{-1/2}e^{(-\Delta G^*/RT)} \quad (6)$$

$$E_{max} = \Delta E_0 + \chi \quad (5)$$

Ground State. The ground state of the mixed-valent $^1/_2$met site can be described by the spin Hamiltonian given in eq 7, which operates over the uncoupled basis set $|S_{Fe^{2+}}, S_{Fe^{3+}}, m_{s_{Fe^{2+}}}, m_{s_{Fe^{3+}}}\rangle$ with the resulting dimer wave functions expressed as $|S_{tot}, \pm m_s\rangle$.

$$\hat{H} = -2J\hat{S}_{Fe^{2+}}\cdot\hat{S}_{Fe^{3+}} + D_{Fe^{2+}}(\hat{S}^2_{zFe^{2+}} - 2) + E_{Fe^{2+}}(\hat{S}^2_{xFe^{2+}} - \hat{S}^2_{yFe^{2+}}) + D_{Fe^{3+}}(\hat{S}^2_{zFe^{3+}} - {}^{35}/_{12}) + g_{zFe^{2+}}\beta H_z\hat{S}_{zFe^{2+}} + g_{xFe^{2+}}\beta H_x\hat{S}_{xFe^{2+}} + g_{yFe^{2+}}\beta H_y\hat{S}_{yFe^{2+}} + g_{zFe^{3+}}\beta H_z\hat{S}_{zFe^{3+}} + g_{xFe^{3+}}\beta H_x\hat{S}_{xFe^{3+}} + g_{yFe^{3+}}\beta H_y\hat{S}_{yFe^{3+}} \quad (7)$$

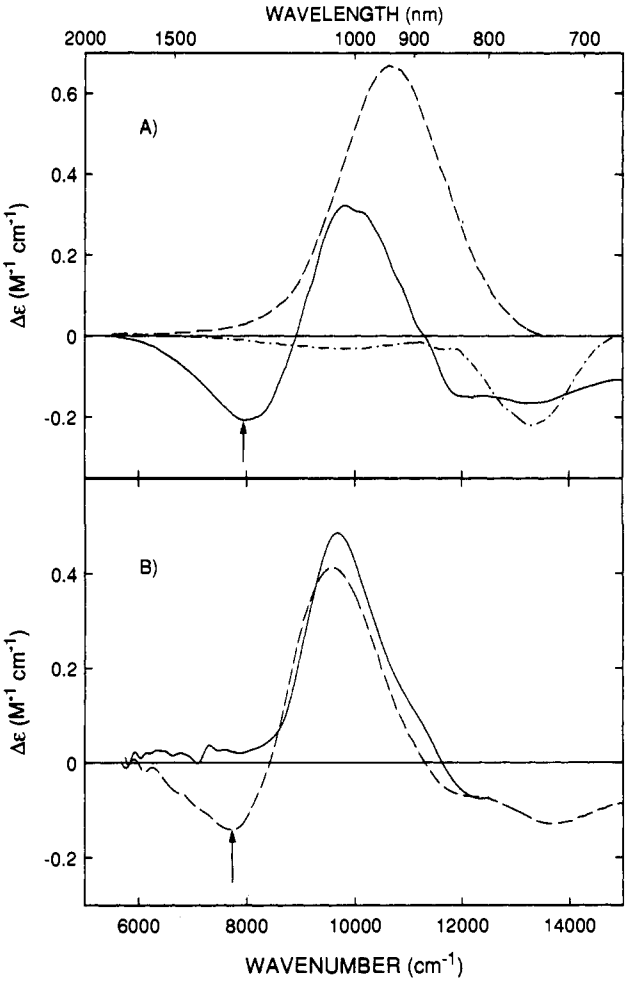

Figure 11. (A) Comparison of the CD spectrum of deoxyN$_3^-$ (--), $^1/_2$metN$_3^-$ (—), and metN$_3^-$ (—·—) at 300 K. (B) Comparison of the $^1/_2$metCl$^-$ CD spectrum at 300 K (--) and 4.20 K (—).

Included in eq 7 is the exchange coupling parameter J[81] as well as axial ($D_{Fe^{2+},Fe^{3+}}$) and rhombic ($E_{Fe^{2+}}$) zero field splitting (ZFS) terms and Zeeman terms ($g_{zFe^{2+}}\beta H_z\hat{S}_{zFe^{2+}}$, etc.).[82] The single site $g_{Fe^{2+}}$ can be coupled to the ZFS parameters using ligand field theory as given in eqs 8a and b, where λ_0 is the Fe^{2+} spin orbit coupling constant (−100 cm^{-1}), and k^2 is the Stevens orbital reduction factor.[83] The sign of $D_{Fe^{2+}}$ is defined by the splitting of the $^5T_2$ ground state such that when the $d_{xz,yz}$ orbitals are below

$$D_{Fe^{2+}} = (-k^2\lambda_o/4)(g_{xFe^{2+}} + g_{yFe^{2+}} - 2g_{zFe^{2+}}) \quad (8a)$$

$$E_{Fe^{2+}} = (-k^2\lambda_o/4)(g_{yFe^{2+}} - g_{xFe^{2+}}) \quad (8b)$$

the d_{xy} orbital (^{5}E ground state) $D_{Fe^{2+}}$ is negative, and with the reversed ordering giving a positive $D_{Fe^{2+}}$ ($^5B_2$ ground state). When $D_{Fe^{2+}}$ is negative, it is necessary to account for spin-orbit coupling within the ^{5}E ground state but this is not included in eqs 8a and b.[84] Thus these equations will give inaccurate $g_{Fe^{2+}}$ for negative $D_{Fe^{2+}}$. They can still be used to get insight, but with the cavaet that the $g_{Fe^{2+}}$ may be inaccurate. For positive values of $D_{Fe^{2+}}$ eqs 8a and b are appropriate.

Application of eq 7 results in a 30 × 30 matrix. Diagonalization of this matrix in zero field with $D_{Fe^{3+}} = E_{Fe^{2+}} = 0$ cm^{-1} gives the

(79) (a) Kestner, N. R.; Logan, J.; Jortner, J. *J. Phys. Chem.* **1974**, *78*, 2148–2166. (b) Hopfield, J. *Proc. Natl. Acad. Sci. U.S.A.* **1974**, *71*, 3640–3644.

(80) The approximation of a symmetric dimer is used to obtain a magnitude of k_{et}.

(81) A positive value of J indicates ferromagnetic coupling, whereas a negative value is antiferromagnetic coupling.

(82) Rotation of the Fe^{3+} ZFS tensor relative to that of the Fe^{2+} was not included in this analysis as the MCD and EPR are not particularly sensitive to this. The orientation of the Fe^{2+} ZFS will thus determine the principal axes of the dimer.

(83) Ballhausen, C. J. *Molecular Electronic Structures of Transition Metal Complexes*; McGraw-Hill: London, 1979; pp 67–78.

(84) Whittaker, J. W.; Solomon, E. I. *J. Am. Chem. Soc.* **1988**, *110*, 5329–5339.

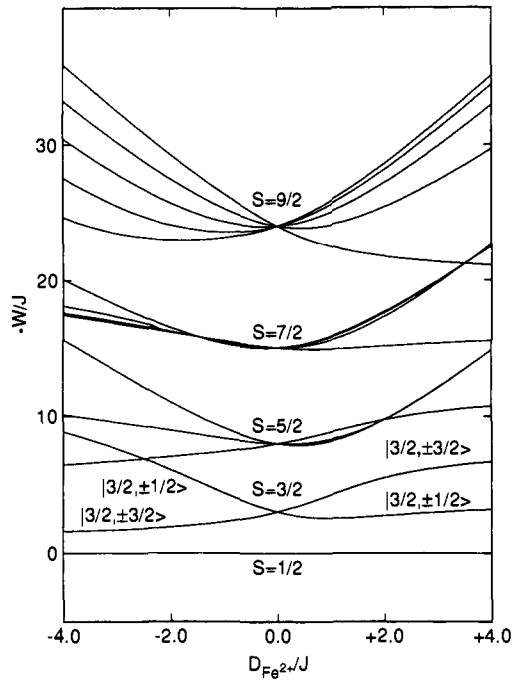

Figure 12. Energy level diagram for a mixed-valent dimer with coupled $S = {}^5/_2$ and $S = 2$ predicted by eq 7. The m_s components of the $S_{tot} = {}^3/_2$ are also indicated. The energy of the $S_{tot} = {}^1/_2$ ground state has been set to zero.

Table V. Ground-State Spin Hamiltonian Parameters

	1/2metN$_3^-$	1/2met$_r$	1/2met$_o$
J (cm^{-1})	−7.6 ± 0.6	−9 ± 1	−7 ± 1
$D_{Fe^{2+}}$	−6.3 ± 0.8	−7.4 ± 0.6	+3.2 ± 0.9
$\|E_{Fe^{2+}}\|$	0.8 ± 0.1	0.91 ± 0.07	0.0
$D_{Fe^{3+}}$	0.8 ± 0.2	0.67 ± 0.06	0.3 ± 0.3
$g_{x,yFe^{2+}}$	2.09 ± 0.01	2.06 ± 0.01	2.14 ± 0.01
$g_{y,xFe^{2+}}$	2.05 ± 0.01	2.01 ± 0.01	2.14 ± 0.01
$g_{zFe^{2+}}$	2.24 ± 0.01	2.225 ± 0.003	2.068 ± 0.004
k^2	0.8 ± 0.2	0.78 ± 0.03	0.85 ± 0.07

energy level diagram in Figure 12, where the energy is given in the reduced energy parameter W/J as a function of $D_{Fe^{2+}}/J$.[85] Of particular interest is the ZFS splitting of the $S_{tot} = {}^3/_2$ first excited state of the dimer as the VT MCD is most sensitive to this state. For negative $D_{Fe^{2+}}$, the $|{}^3/_2, \pm{}^1/_2\rangle$ state is lowest in energy, while for positive $D_{Fe^{2+}}$ the $|{}^3/_2, \pm{}^3/_2\rangle$ is lowest (see Figure 12).[86,87]

The dimer g values are sensitive to both $D_{Fe^{2+}}$ and J, as shown in Figure 13.[88] For J large relative to $D_{Fe^{2+}}$ (i.e., $J = -100$ cm^{-1} in Figure 13C), the dimer g values have a linear dependence of $D_{Fe^{2+}}$ (and $g_{Fe^{2+}}$), as predicted by a simple vector coupling of spins.[89-91] However when J becomes comparable to $D_{Fe^{2+}}$ (Figure 13A,B), the dimer g values deviate from this simple behavior. The deviation is caused by interaction of the $|{}^1/_2, \pm{}^1/_2\rangle$ ground state with the $S_{tot} = {}^3/_2$ states which increases as the energy to these states become smaller (Figure 12). This effect is pronounced when $D_{Fe^{2+}}$ is negative and the $|{}^3/_2, \pm{}^1/_2\rangle$ is lowest in energy. The $|{}^3/_2, \pm{}^3/_2\rangle$ can interact only weakly with the $|{}^1/_2, \pm{}^1/_2\rangle$ ground state, thus for positive $D_{Fe^{2+}}$ the deviation from linear behavior is small.[92] The ordering of the dimer g values for positive $D_{Fe^{2+}}$ is always $g_\parallel > g_\perp$, but for $D_{Fe^{2+}}$ negative the ordering is reversed, except for very small J (Figure 13A). The fact that ${}^1/_2$met$_o$ has the dimer $g_\parallel > g_\perp$ indicates $D_{Fe^{2+}}$ for ${}^1/_2$met$_o$ is positive. For ${}^1/_2$met$_r$ and ${}^1/_2$metN$_3^-$ the order of the dimer g values is opposite that of ${}^1/_2$met$_o$ (dimer $g_\perp > g_\parallel$) indicating $D_{Fe^{2+}}$ is negative.

Table V gives the values of the ZFS and Zeeman parameters for each iron and the J of the dimer obtained by fitting eq 7 to the experimental W_1 and the dimer g values (Table III) using a simplex routine.[55] In the fit, J, $g_{yFe^{2+}}$, $g_{zFe^{2+}}$, and $E_{Fe^{2+}}$ were

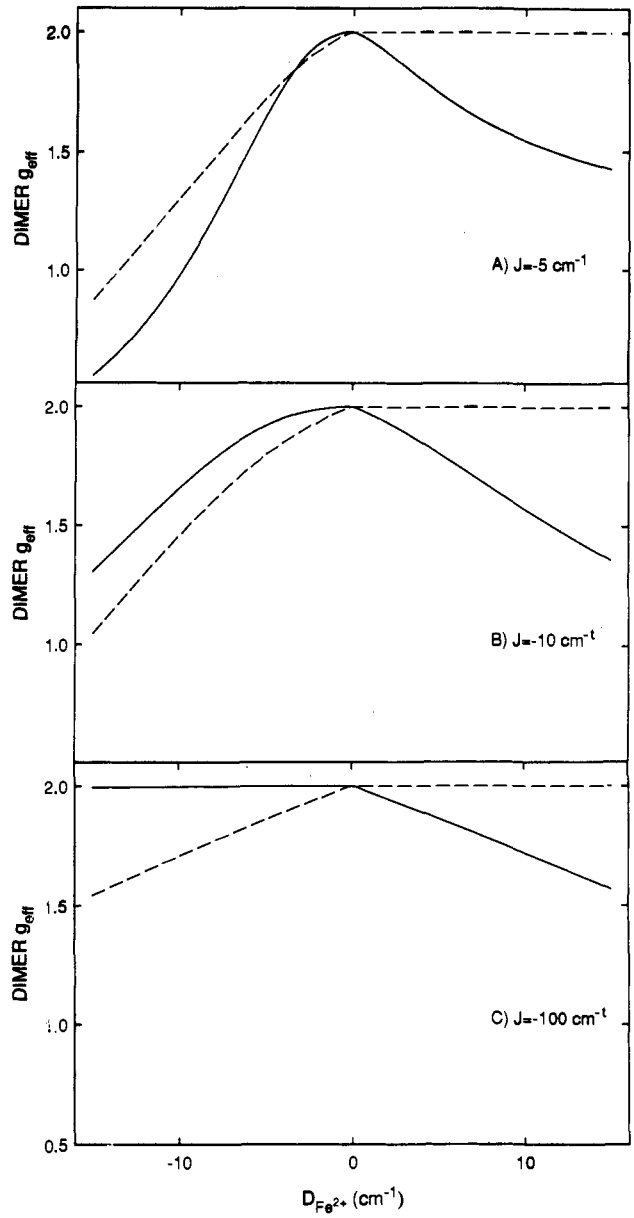

Figure 13. Dependence of the dimer $g_\parallel$ (−−) and $g_\perp$ (—) on $D_{Fe^{2+}}$) for (A) $J = -5$ cm^{-1}, (B) $J = -10$ cm^{-1}, and (C) $J = -100$ cm^{-1}.

(85) For positive values of J, the diagram needs only to be inverted making $S_{tot} = {}^9/_2$ the ground state.

(86) This is the same result obtained by a perturbational approach, which solved the problem in the coupled basis set neglecting contributions from states above $S_{tot} = {}^3/_2$. Both methods predict nearly identical energies for the $S_{tot} = {}^3/_2$ components in zero field for small $D_{Fe^{2+}}/J$. When $D_{Fe^{2+}}/J \geq 1$ components of the $S_{tot} = {}^5/_2$ state are now low enough in energy to interact with the $S_{tot} = {}^3/_2$ state.[87]

(87) Guigliarelli, B.; Bertrand, P.; Gayda, J. P. *J. Chem. Phys.* **1986**, *85*, 1689–1692.

(88) For the plots shown in Figure 13, when $D_{Fe^{2+}}$ is negative, $g_{\perp Fe^{2+}}$ was fixed at 2.00, and when $D_{Fe^{2+}}$ is positive, $g_{\perp Fe^{2+}}$ was held equal to 2.00 and the other $g_{Fe^{2+}}$ were determined using eq 8a. The values of $E_{Fe^{2+}}$, and $D_{Fe^{3+}}$ were set equal to zero and k^2 was held equal to 1.0, so as to separate their effects on the dimer g values from those of $D_{Fe^{2+}}$ and J. The orbital reduction factor causes a decrease in the dimer g values as it is allowed to deviate from 1.0. $E_{Fe^{2+}}$ splits the dimer $g_\perp$ and causes all dimer g values to decrease. The effect of $D_{Fe^{3+}}$ on the dimer g values is small and is approximately additive to that of $D_{Fe^{2+}}$.

(89) Bertrand, P.; Guigliarelli, B.; Gayda, J. P. *Arch. Biochem. Biophys.* **1986**, *245*, 305–307.

(90) A simple vector coupling of the g tensors ($\bar{g}$) of an $S = {}^5/_2$ and $S = 2$ gives the equation $g_{dimer} = ({}^7/_3)\bar{g}_{Fe^{3+}} - ({}^4/_3)\bar{g}_{Fe^{2+}}$.[87,89,91]

(91) Gibson, J. F.; Hall, D. O.; Thornley, J. H. M.; Whatley, F. R. *Proc. Natl. Acad. Sci. U.S.A.* **1966**, *56*, 987–990.

(92) With $D_{Fe^{2+}}$ positive the dimer g is unaffected by changes in $D_{Fe^{2+}}$, but it is affected by deviation of the $g_{Fe^{2+}}$ from 2.00. Allowing the single site $g_{Fe^{2+}}$ values to deviate above 2.00 decreases the dimer g values for both $D_{Fe^{2+}}$ positive and negative.

adjustable parameters; $g_{xFe^{2+}}$ and $D_{Fe^{2+}}$ were determined from $g_{yFe^{2+}}$, $g_{zFe^{2+}}$, and $E_{Fe^{2+}}$ using eqs 8a and b. Depending on the sign of $D_{Fe^{2+}}$ either $g_{yFe^{2+}}$ or $g_{zFe^{2+}}$ was initially held equal to 2.00 but allowed to float in later refinements. The sign of $D_{Fe^{2+}}$ was determined from the EPR data and its magnitude was constrained to be less than the maximum observed for Fe^{2+} (± 15 cm^{-1}).[93] $E_{Fe^{2+}}$ was constrained so $|E_{Fe^{2+}}/D_{Fe^{2+}}| \leq 1/3$ (for $^1/_2$met$_o$ ($E_{Fe^{2+}} = 0.0$ cm^{-1})).[94] The orbital reduction factor on the Fe^{2+} was initially set to 0.80 but was allowed to vary in the final fits. The $g_{Fe^{3+}}$ were set equal to 2.00 and were not adjusted, but $D_{Fe^{3+}}$ was an adjustable parameter constrained to be ≤ 1 cm^{-1}.

All three $^1/_2$mets have $J \approx -8$ cm^{-1}, consistent with the presence of a μ-OH$^-$ bridge, as suggested earlier for $^1/_2$metN$_3^-$.[19,29] Note that the previous studies used indirect methods to measure J and ignored the ZFS terms in eq 7.[95,96] The only other system where a direct measurement of J has been made is the mixed-valent form of uteroferrin (Uf),[97] and our results would indicate that $^1/_2$metHr and the non-phosphate bound $^1/_2$metUf are quite similar. The major difference in the ground-state parameters between the three $^1/_2$mets found from this analysis is in the sign of $D_{Fe^{2+}}$, which for $^1/_2$met$_r$ and $^1/_2$metN$_3^-$ is negative but for $^1/_2$met$_o$ is positive (see Table V). This parallels the results of our excited-state studies which have shown that $^1/_2$met$_o$ has a very different coordination geometry around the Fe^{2+} as compared to $^1/_2$met$_r$ and $^1/_2$metN$_3^-$. This analysis also indicates that the variations in the dimer g_{eff} values for the $^1/_2$metL$^-$ series (Table S1) are primarily due to changes in the ZFS on the Fe^{2+}, as J is about the same for all $^1/_2$metL$^-$.[98]

pH Dependence. Comparison of the pH 6.0 EPR data (Figures 8 and 9) to that of $^1/_2$met$_r$ and $^1/_2$met$_o$ in Figure 5 identifies the predominant $^1/_2$met product at pH 6.0 as $^1/_2$met$_o$. $^1/_2$Met$_o$ is the final mixed-valent product of both the oxidation and reduction at pH 6.0. A similar comparison of the pH 8.2 and pH 9.0 EPR spectra (Figures 8 and 9) identifies the high pH $^1/_2$met product as predominantly $^1/_2$met$_r$, and again the same final equilibrium mixture is achieved by either oxidation or reduction. The data at pH 7.0, given in Figure 8, show that at this pH both $^1/_2$met$_r$ and $^1/_2$met$_o$ are present. Both the reduction at pH 7.0 followed by dialysis into different pH buffers and the direct reduction/oxidation at high (pH 9.0) and low pH (pH 6.0) show the $^1/_2$met$_r$ and $^1/_2$met$_o$ interconversion is a pH-dependent equilibrium ($pK_a \approx 7.6$) with $^1/_2$met$_o$ the low pH and $^1/_2$met$_r$ the high pH form.[99]

Discussion

The ABS, CD, and LT MCD spectral studies on the $^1/_2$metHr site have shown that all exogenous ligands bind to the Fe^{3+} and

Scheme I

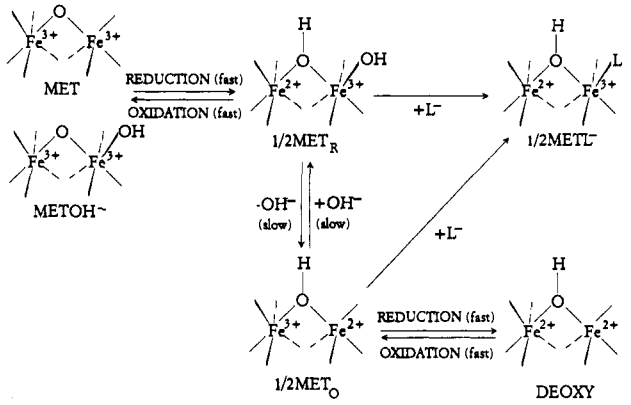

that $^1/_2$met$_r$ and the $^1/_2$metL$^-$ derivatives have very similar ligand field CD and LT MCD spectra. Both $^1/_2$met$_r$ and $^1/_2$metL$^-$ show two Fe^{2+} ligand field bands at $\sim$10 000 cm^{-1}, with a Δ^5E of 2000 cm^{-1} indicating a six-coordinate Fe^{2+}. In addition, the Fe^{3+} ligand field bands in these species occur at $\sim$11 000 cm^{-1} ($^6A_1 \rightarrow {}^4T_1$) and at $\sim$14 000 cm^{-1} ($^6A_1 \rightarrow {}^4T_2$), indicative of a six-coordinate Fe^{3+}. The spectral studies show that $^1/_2$met$_o$ is very different from $^1/_2$met$_r$ and $^1/_2$metL$^-$ with a very large splitting of the Fe^{2+} ligand field bands ($\Delta^5E \approx 5000$ cm^{-1}). This large Δ^5E, the change in sign of $D_{Fe^{2+}}$ from the VT MCD and EPR analysis, and the larger reorganizational energy from the IT analysis indicate that there is a five-coordinate Fe^{2+} in $^1/_2$met$_o$. The observation of the Fe^{3+} $^6A_1 \rightarrow {}^4T_2$ ligand field bands at $\sim$14 000 cm^{-1} indicates that the Fe^{3+} is six-coordinate. The VT MCD gives a magnitude of the antiferromagnetic coupling between the irons of $\sim$8 cm^{-1} for all $^1/_2$met species, consistent with the presence of a bridging OH$^-$. As the coupling is the same for $^1/_2$met$_r$ and $^1/_2$met$_o$, the observed pH-dependent equilibrium of these two species cannot involve the bridge. This equilibrium and the spectral analysis which shows that $^1/_2$met$_r$ has an additional ligand relative to $^1/_2$met$_o$, indicates that $^1/_2$met$_r$ has a H_2O derived bound exogenous ligand which is not present in $^1/_2$met$_o$. Since H_2O is not known to bind to metHr[8,12-14] or deoxyHr,[7] but OH$^-$ does bind to met at high pH,[8,12-14] the exogenous ligand is most likely OH$^-$. The proposed active site structures for the $^1/_2$metHr species examined in this study and their interconversions are shown in Scheme I.[100] Note that in Scheme I, the binding of an exogenous ligand to the open coordination site in $^1/_2$met$_o$ induces an intramolecular electron transfer from the 2-His Fe to the 3-His Fe.[19,28]

It has been suggested that the difference between $^1/_2$met$_r$ and $^1/_2$met$_o$ and the different redox behavior of these two species results from where the redox agent is able to access the site (i.e., the 3-His Fe could be the site of both oxidation and reduction as it is closest to the protein surface).[19] The IT analysis shows that the rate of intramolecular electron transfer is very rapid ($k \approx 10^8$ s^{-1}, Table IV). Since this rate is faster than the observed rates for reduction of met/metOH$^-$ ($k \approx 10^6$ M^{-1} s^{-1})[17-19,23] or the oxidation of deoxy ($k \approx 10^5$ M^{-1} cm^{-1}),[23] the electron cannot be kinetically trapped and the localization must reflect a thermodynamic preference. In addition, the intramolecular electron transfer cannot be the rate-limiting step in the slow interconversion ($k \approx 10^{-3}$ s^{-1}) of the two $^1/_2$mets. The slow pH-dependent interconversion of $^1/_2$met$_r$ and $^1/_2$met$_o$ most likely reflects the binding of the exogenous OH$^-$, similar to the pH-dependent interconversion of metOH$^-$ and met.[101]

The structures of $^1/_2$met$_r$ and $^1/_2$met$_o$ in Scheme I also give insight into the different reactivities of the $^1/_2$met site as well as the observed redox reactivities of met and deoxy. Also given in Scheme I are the known redox reactions of Hr along with the structures of the species present at each oxidation level. Reduction

(93) (a) Rudowicz, C. *Acta Phys. Pol.* **1975**, *A47*, 305–321. (b) Champion, P. M.; Sievers, A. J. *J. Chem. Phys.* **1977**, *66*, 1819–1825.

(94) The data for $^1/_2$met$_o$ could not be fit to a negative value of $D_{Fe^{2+}}$. In addition, constraining $D_{Fe^{2+}}$ for $^1/_2$metN$_3^-$ or $^1/_2$met$_r$ to be positive gave an unreasonable $E_{Fe^{2+}}/D_{Fe^{2+}}$.

(95) The temperature-dependent paramagnetic NMR gave values of J of -10 and -20 cm^{-1}, depending on which resonance was monitored[29] and should be considered to give an order of magnitude estimate for J. The temperature-dependent EPR studies measured the line width of the EPR signal and assumed an Orbach relaxation mechanism to place the first excited state at 45 cm^{-1}, as compared to the VT MCD results in Table II of $\sim$20 cm^{-1}. The higher estimate for the energy of the first excited state does not affect the conclusions reached here, as fitting eq 7 with the higher energy changes J to ~ -17 cm^{-1}, which is still within the range expected for a OH$^-$ bridge.[96]

(96) The results of fitting eq 7 for $^1/_2$metN$_3^-$ with $W_1 = 45$ cm^{-1} are as follows: $J = -17.0 \pm 1$ cm^{-1}, $D_{Fe^{2+}} = -7.1 \pm 0.1$, $|E_{Fe^{2+}}| = 0.94 \pm 0.02$ cm^{-1}, $D_{Fe^{3+}} = 0.52 \pm 0.04$ cm^{-1}, $k^2 = 0.80 \pm 0.01$, $g_{y,xFe^{2+}} = 2.123 \pm 0.002$, $g_{x,yFe^{2+}} = 2.076 \pm 0.002$, and $g_{zFe^{2+}} = 2.278 \pm 0.004$.

(97) (a) Day, E. P.; David, S. S.; Peterson, J.; Dunham, W. R.; Bonvoisin, J. J.; Sands, R. H.; Que, L., Jr. *J. Biol. Chem.* **1988**, *263*, 15561–15567. (b) Sage, J. T.; Xia, Y. M.; Debrunner, P. G.; Keough, D. T.; deJersey, J.; Zerner, B. *J. Am. Chem. Soc.* **1989**, *111*, 7239–7247.

(98) A previous study concluded that changes in the $E_{Fe^{2+}}$ ZFS parameter were responsible for the observed EPR changes.[87] However, this analysis assumed that the dimer g values could be related to the single site g values by a simple vector coupling of spins. This is not appropriate when $D_{Fe^{2+}}$ and J are comparable (see Figure 13A,B) and leads to the wrong sign of $D_{Fe^{2+}}$ as well as $|E_{Fe^{2+}}/D_{Fe^{2+}}| > 1/3$.

(99) It has been possible to measure the pH-dependent equilibrium between $^1/_2$met$_r$ and $^1/_2$met$_o$ because Hr from *P. gouldii* disproportionates much less ($\sim$10–20%) relative to Hr from other species (e.g., Hr from *T. zostericola* disproportionates completely).[17d,20a,23]

(100) Scheme I does not include disproportionation, although it is an important process in the redox chemistry of Hr (see Figures S6–S10 and Table S2).[17-19,23-25]

(101) Bradić, Z.; Wilkins, R. G. *Biochemistry* **1983**, *22*, 5396–5401.

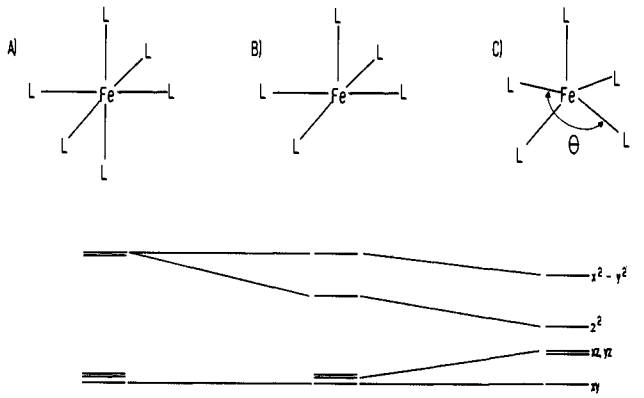

Figure 14. Energy diagram showing the effects on (A) the d orbitals of an octahedral Fe^{2+} caused by (B) removing one ligand to give a square-pyramidal complex and (C) raising the Fe^{2+} above the basal ligand plane with the angle between the basal ligands of Θ.[106]

of both met and $metOH^-$ gives $^1/_2met_r$, requiring the protonation of the oxo bridge and in the case of met, introduction of an exogenous OH^-. The lack of a deuterium isotope effect in the reduction of met[19] indicates protonation of the bridge is not the rate-limiting step. Thus, the fast rate of reduction requires a mechanism for rapid protonation of the bridge and binding of exogenous OH^-, perhaps in a concerted mechanism. The rapid reduction[18,23] of $metOH^-$ requires that, unlike the other $metL^-$,[102] OH^- does not dissociate before reduction. The OH^- may thus provide a mechanistic route for protonation of the oxo bridge. One possibility is a concerted protonation of the bridge through the exogenous OH^-, which hydrogen bonds to the oxo bridge.[12i] Oxidation of $^1/_2met_r$ to met or $metOH^-$ is then rapid because the OH^- assists in the deprotonation of the bridging OH^-. However further reduction of $^1/_2met_r$ is slow because the OH^- must dissociate as deoxy has no bound exogenous ligand. Deoxy and $^1/_2met_o$ have a bridging OH^- and a five-coordinate Fe^{2+}, so there will be little structural rearrangement necessary to go from one to the other, and the rates of the redox reactions will be fast. Oxidation of $^1/_2met_o$ will be slow, proceeding through the slow binding of OH^- to give $^1/_2met_r$, which is quickly oxidized.[103]

The IT analysis shows a large ΔE_0 for $^1/_2met_r$ and $^1/_2met_o$ (Table IV), indicating the potential surface for the localization of the extra electron on one Fe is much lower in energy than for the electron on the other Fe. The large ΔE_0 for $^1/_2met_r$ indicates the electron is localized on the 3-His Fe, even though both irons are six-coordinate. The added stability of the 3-His Fe may be due either to the presence of the extra imidazole or perhaps the 3-His Fe is structurally capable of distorting so as to better accommodate the longer Fe^{2+} bond lengths. For $^1/_2met_o$ the extra electron is localized on the 2-His Fe, likely resulting from the lower ligand-electron repulsion in a five-coordinate structure as predicted by crystal field theory. In the formalism of Companion and Komarynsky,[104] an octahedral ligand field raises the d orbital energy by $6\alpha_0$,[105] but a five-coordinate ligand field will raise the d orbitals by only $5\alpha_0$. It is thus more energetically favorable for the extra electron to be localized on the center with the smaller ligand-electron repulsion.

The Fe^{2+} ZFS in the $^1/_2met$ sites gives additional insight into the ligand geometry around the Fe^{2+}. The negative $D_{Fe^{2+}}$ for the six-coordinate Fe^{2+} in $^1/_2metL^-$, indicates the degenerate e set of d orbitals is lowest in energy.[84] A $d_{xz,yz}$ ground state requires a weak ligand along the axial direction of the octahedron. This weak ligand is probably the bridging OH^- as it is expected to be distorted toward the more oxophilic Fe^{3+}. The positive sign of $D_{Fe^{2+}}$ for the five-coordinate Fe^{2+} in $^1/_2met_o$ can be interpreted based on the extended Hückel treatment of five-coordinate metal complexes of Rossi and Hoffmann.[106] Removal of an axial ligand from an octahedral complex (Figure 14A) in the absence of π bonding, causes the d_{z^2} orbital to drop in energy (Figure 14B). Raising the metal out of the basal ligand plane (Figure 14C) causes the $d_{xz,yz}$ set to go up in energy relative to the d_{xy} orbital (dependent on the angle Θ between a pair of trans basal ligands). This d orbital splitting diagram corresponds to a positive $D_{Fe^{2+}}$. This model predicts the strongest metal–ligand σ bond is with the ligand in the apical position of the puckered square pyramid. The bridging OH^- cannot be the strong axial ligand in $^1/_2met_o$ for the reason stated above. The increased delocalization found for $^1/_2met_o$ as compared to $^1/_2metL^-$ in the IT analysis suggests that $^1/_2met_o$ has a better pathway for electron delocalization (i.e., better overlap of the orbital containing the extra electron (d_{xy}) and the orbitals on the OH^- bridge), which also requires that the bridging OH^- does not define the molecular z axis in $^1/_2met_o$.

The spectroscopic protocol developed here has given insight into the structure and reactivity of the $^1/_2metHrs$. It is especially useful in determining the coordination geometries around each iron in the active site and in defining bridging ligation. It will now be important to extend this protocol to other mixed-valent binuclear non-heme iron systems, such as the purple acid phosphatases and methane monoxygenase.

Acknowledgment. We thank NSF Grant DMB9019752 for support of this research.

Registry No. OH^-, 14280-30-9.

Supplementary Material Available: Tables giving the dimer g values of various $^1/_2met$ species and concentrations of met, oxy, and $^1/_2met$, additional spectra of $^1/_2met$ species, Gaussian fits of the ligand field region of $^1/_2metCl^-$, $^1/_2metN_3^-$, $^1/_2met_r$, and $^1/_2met_o$, and material (table, kinetic traces, and spectra) related to the pH-dependent conversion of $^1/_2met_r$ and $^1/_2met_o$ (14 pages). Ordering information is given on any current masthead page.

(102) Olivas, E.; deWaal, D. J. A.; Wilkins, R. G. *J. Inorg. Biochem.* **1979**, *11*, 205–212.

(103) It should be noted that $^1/_2met_o$ from *P. gouldii* has been reported to be directly oxidized to met at a rate of $1.7 \times 10^2\ M^{-1}\ s^{-1}$ (pH 6.0) which is slower than the oxidation of $^1/_2met_r$ ($3.4 \times 10^2\ M^{-1}\ s^{-1}$ at pH 8.2).[23] This may require a direct deprotonation of the endogenous OH^- bridge.

(104) Companion, A. L.; Komarysnky *J. Chem. Ed.* **1964**, *41*, 257–262.

(105) Neglecting overlap of the metal and ligand orbitals, the α_0 parameter of Companion and Komarysnky is defined by

$$\alpha_0 = Ze^2\left[\frac{1}{R}\int_0^R (R_{3d})^2 r^2 dr\right]$$

where R is the metal ligand distance, r is the distance from the electron to the nucleus, and Ze is the negative charge on the ligand.[104]

(106) Rossi, A. R.; Hoffmann, R. *Inorg. Chem.* **1975**, *14*, 365–374.